A FINITE ELEMENT MODEL OF A REALISTIC FOOT AND ANKLE FOR FLATFOOT ANALYSIS

by

Lindsey Leigh Williams

_____

A Thesis Submitted to the Faculty of the

DEPARTMENT OF AEROSPACE AND MECHANICAL ENGINEERING

In Partial Fulfillment of the Requirements

For the Degree of

MASTER OF SCIENCE

WITH A MAJOR IN MECHANICAL ENGINEERING

In the Graduate College

THE UNIVERSITY OF ARIZONA

2017

STATEMENT BY AUTHOR

The thesis titled A Finite Element Model of a Realistic Foot and Ankle for Flatfoot Analysis prepared by Lindsey Williams has been submitted in partial fulfillment of requirements for a master's degree at the University of Arizona and is deposited in the University Library to be made available to borrowers under rules of the Library.

Brief quotations from this thesis are allowable without special permission, provided that an accurate acknowledgement of the source is made. Requests for permission for extended quotation from or reproduction of this manuscript in whole or in part may be granted by the head of the major department or the Dean of the Graduate College when in his or her judgment the proposed use of the material is in the interests of scholarship. In all other instances, however, permission must be obtained from the author.

SIGNED: Lindsey Williams

APPROVAL BY THESIS DIRECTOR

This thesis has been approved on the date shown below:

_____ _____

L. Daniel Latt, MD PhD Date

Associate Professor

Orthopaedic Surgery and Biomedical Engineering

ACKNOWLEDGEMENTS

I would like to thank:

- Dr. Daniel Latt and Dr. Erdogan Madenci for their generous help and support. I appreciate their valuable time, guidance, and recommendations.
- Committee member Dr. John Szivek for his time and insightful suggestions.
- Eric Lintula from Paragon 28 for his time and recommendations to advance the project.
- Cody Mitts and Evan Willmarth for helping create the geometry and giving valuable advice.
- Rafael Bernal, Mehmet Dorduncu, Yile Hu, and Scott Harrison for their support.
- Dr. Samy Missoum for his thoughtful comments and suggestions.
- Joe Shaffer, Dustin Boesch, Jeremy Gustin, and Taylor Wender from Quartus Engineering for their valuable time and support for troubleshooting the model.
- Hari Subramanium from ANSYS for his time and suggestions.
- Foot & Ankle Orthopaedics for publishing the model on their journal cover.
- Paragon 28 and the University of Arizona for the financial support.
- My parents Don and Peggy Conklin, my sister Megan Clarke, and my husband Jacob Williams for their continuous love, patience, and support.

TABLE OF CONTENTS

LIST OF FIGURES

LIST OF TABLES

1. ABSTRACT

Adult-Acquired Flatfoot is a degenerative condition in which the ligaments and tendons supporting the arch deteriorate eventually leading to arch collapse. This deterioration can occur at various locations along the arch creating a number of different patterns of collapse. Surgical treatment for adult acquired flatfoot consists of a combination of various osteotomies. Although general guidelines exist, there is no systematic way to determine which combination of osteotomies should be used to correct a given foot deformity. Computer simulation with finite element analysis might provide an analytical tool to optimize the choice of osteotomy location and size. By dividing a complex problem into simpler components, finite element analysis allows for the solution of complex problems by solving a large set of simple equations.

Finite element analysis has previously been used to study effects of diabetes, shoe design, and gait analysis in the foot. These studies have oversimplified geometry and material properties of foot tissues which limits the true mechanical behavior. The goal of this study was to create an anatomically and physiologically correct finite element model of the foot and ankle.

To create a healthy foot model, CT scans were collected from one cadaver foot to create a three-dimensional cortical bone model in 3D Slicer software. The cortical bone model was imported into SolidWorks to create the geometry for trabecular bone, cartilage, ligaments, and tendons. Journal articles, textbooks, and other resources were used in order to create realistic cartilage, ligament, and tendon models (Netter & Colacino, 1997; see also Boss & Hintermann, 2002; Campbell et al., Apr. 2014; Golanó et al., 2010; Mahadevan). Final approval of the model's geometry was obtained from the orthopaedic surgeon supervising this study. After completing the anatomically correct geometry of the foot, it was imported into finite element software (ANSYS, http://www.ansys.com/). The model was meshed with solid elements only: tetrahedral elements for the foot and hexahedral elements for the ground support. Linear elastic material properties were assigned to all bodies. Boundary conditions and contacts were created including a fixed ground support and bonded and frictionless contacts. A body weight force was applied to the tibia and tendon forces were applied to simulate loading during midstance.

The frictionless contacts created a nonlinear problem that caused the simulation to fail to converge to a solution. Abnormally high stresses and deformation were found in the results. The foot model failed to converge to realistic results because of the current model's complexity.

An anatomically correct foot model was successfully created, but simplifications need to be made to the model in the future for convergence. Recommendations for simplification include modeling ligaments as truss elements, adding spring elements to tendons, and adding soft tissue or fat pads to the model. After simplifications are completed and realistic results are obtained, Flatfoot conditions and surgeries can be simulated and analyzed.

2. BACKGROUND

Adult-Acquired Flatfoot is a progressive condition where the arch collapses in the foot due to the attenuation of the supporting ligaments and tendons. Surgery is often used to treat Flatfoot with the goal of addressing each of the many malalignments, but the current surgical guidelines are limited. The complex, multi-planar interplay of the malalignments creates a difficult process for which osteotomies to use. Instead of relying on a quantitative approach to solve a complicated procedure, a quantitative method should be integrated. Surgeons should use a mathematical methodology that recommends a reasonable approach to correcting the malalignments. Finite element analysis provides a possible solution using three-dimensional computer simulation of the foot and ankle. Ideally, a finite element model could aid in the decision-making for the location and size of the osteotomy. A better understanding of the terminology in anatomy of the foot and finite element analysis is necessary and is therefore presented below before describing the methods used in this study.

2.1. Foot Anatomy

2.1.1. Anatomical Coordinates

In order to navigate through the anatomy, there are terms to describe the locations of different structures in the body. Relevant to the foot anatomy, there are four pairings of anatomical terms that are related to the three anatomical planes of the body.

2.1.1.1. Medial and Lateral

One set of terms is medial and lateral which align with the sagittal plane. Medial refers to the anatomical parts that are closer to the midline of the body. Lateral refers to the anatomical parts that are closer to the outer sides of the body. For example, arms are lateral to the chest and big toes are medial to pinky toes (Figure 1). These directional terms are orthogonal to the sagittal plane (Figure 2).

2.1.1.2. Distal and Proximal

Another set of directional terms include distal and proximal which describe how far or close an object is relative to the center of the body. The farther away it is, the more distal it is considered to be. Proximal is the opposite. It refers to the object being closer. Considering the anatomy of the foot the toes are distal to the heel and the heel is proximal to the toes (Figure 1). Depending on what part of the body is referenced, the anatomical plane may change in relation to these terms. In the foot, the coronal (or frontal) plane passes through the foot from the front of the body at the distal end to the back of the body at the proximal end.

Figure 1: Medial, lateral, proximal and distal directional terminology explained using a diagram of the foot (Northcoast Footcare, 2017)

2.1.1.3. Posterior and Anterior

The directional terms anterior and posterior relate how close an object is to the front or back of the body, respectively. Parts of the body that are anterior to the rest of the body include the face and the chest. The posterior part of the body refers to parts such as the back or heel bone. The anatomical plane that moves orthogonally from the front to the back of the body is known as the coronal (or frontal) plane (Figure 2). This plane is shared by the distal and proximal coordinates.

2.1.1.4. Superior and Inferior

The last set of important anatomical coordinates is superior and inferior. Superior refers to being closer to the top of the body i.e. toward the head. Inferior refers to the bottom of the body near the foot. For example, the knee is the superior to the ankle and the heel is inferior to the ankle. The anatomical plane that moves orthogonally from the top to the bottom of the body and is used to reference superior and inferior parts is known as the axial plane (Figure 2).

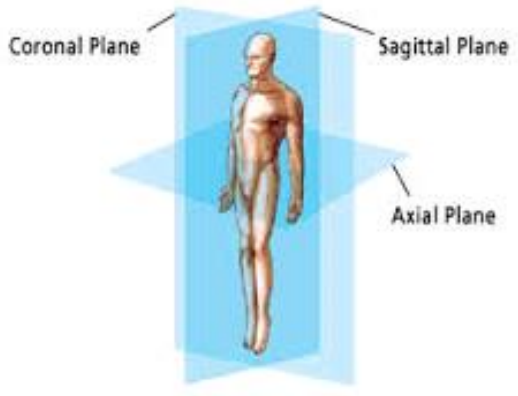

Figure 2: Three anatomical body planes (coronal, sagittal, and axial) explained using a diagram of the human body (Explaining Spinal Anatomy, 2017)

2.1.2. Foot Tissues

In this paper, several different tissues of the body were modeled to represent the anatomy of the foot. The tissues that are important to understand for this study are the bones, cartilage, ligaments, and tendons.

2.1.2.1. Bones

Bones are the source of the body's main structural element. They provide strength and stability for the body's overall framework. The foot can be divided into three sections: the forefoot, midfoot and hindfoot (Figure 3). The forefoot is the most distal part of the foot and consists of the phalanges and the metatarsals. The midfoot is more proximal than the forefoot. The midfoot contains three cuneiforms (medial, intermediate, and lateral), the cuboid, and the navicular. The hindfoot is the most proximal section of the foot and contains the talus and calcaneus. The calcaneus is the heel bone supporting most of the body weight. The talus is superior to the calcaneus making contact with the bones of the lower leg (tibia and fibula). The contact surface between the talus and the bones of the lower leg is known as the ankle. The tibia is significantly larger than the fibula and supports most of an individual's body weight (Figure 4).

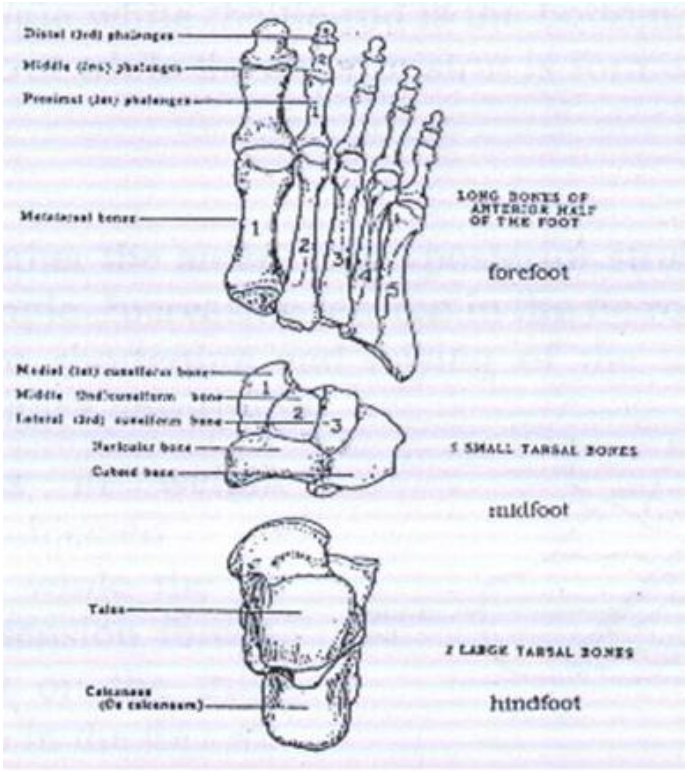

Figure 3: Foot bones categorized into hindfoot (talus, calcaneus), midfoot (cuneiforms, cuboid, and navicular), and forefoot (metatarsals and phalanges) sections (Rose, 2017)

Figure 4: Tibia and fibula bone locations in the lower leg (Fitzgordon, 2016)

Bone is a composite material consisting of collagen, hydroxyapetice, calcium phosphate, calcium carbonate, and water. It exists in two principal forms based the compactness of the organic matrix: cortical bone and trabecular bone (Figure 5,Figure 6, and Figure 7). Cortical bone is the hard bony shell that creates the perimeter of the bone. The thickness of the cortical shell depends on the bone's shape and location. For example, thicker cortical shells occur in the shaft

of a long bone. In contrast, trabecular bone is an irregular, honeycomb structure that creates the inner layer of bone. The honeycomb structure provides shock absorption during impact loading often associated with activities like running or jumping. Trabecular bone, also known as cancellous or spongy bone, is less dense, less stiff, and weaker than cortical bone. Cortical and trabecular bone have two very different sets of the mechanical properties because of their structure and materials properties.

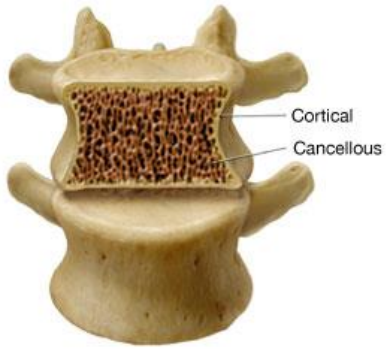

Figure 5: Frontal cross-section of cortical and cancellous (trabecular) bone of vertebrae (Chiro, 2013)

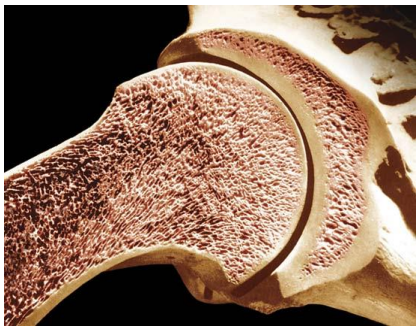

Figure 6: Sagittal cross-section of human femur and pelvis to show cortical and trabecular bone (Compact bone, 2017)

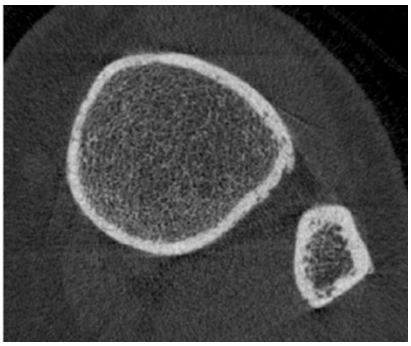

Figure 7: Axial cross-section of tibia and fibula to show difference between cortical and cancellous bone in a CT scan

2.1.2.2. Cartilage

In order to reduce friction between bones, cartilage covers the bone surfaces. Cartilage allows articulation between bones (Figure 8). Articular cartilage is a strong and flexible material that keeps the bones from rubbing against one another which would cause friction and damage to the bones. The cartilage between bones will vary in thickness depending on the magnitude of load transfer in that area. Thicknesses usually range from less than 1 millimeter to as thick as 6 millimeters (Figure 9) in the knee joint (Cohen et al., 1999). In the foot, cartilage thickness is roughly 1 millimeter (Sorrento, 2017).

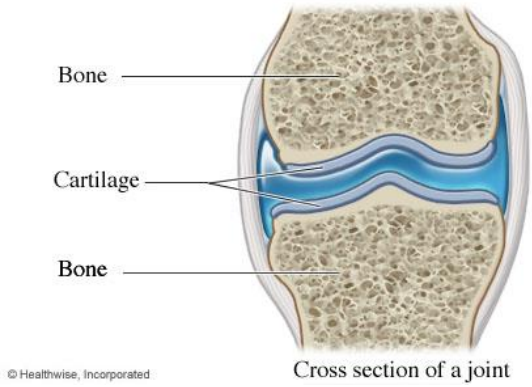

Figure 8: Frontal cross section of a joint showing cartilage between two bones (Blahd & Fu, 2015)

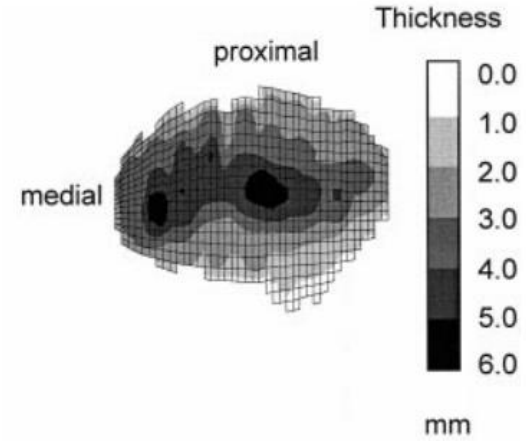

Figure 9: Cartilage thickness maps from in-vivo of a knee joint (Cohen et al., 1999)

2.1.2.3. Ligaments

Ligaments attach from one bone to the other in order to provide stability for joints. Ligaments are made of collagen fibers which provide them with tough and flexible mechanical properties. The length of ligaments will depend on how far the bones are from one another. The attachment areas of the ligament on the bone will vary in cross-sectional area. The two attachment points of the ligaments are referred to as the origin and insertion point. The origin of a ligament is located on the bone that will relatively remain in place and the insertion point is

located on the bone expected to move. In the foot alone, there are over 100 ligaments (Anatomy of the Foot, 2017). The names of the ligaments will depend on the bones they are attached to and their relative position. For example, the talofibular ligament is a ligament attaching from the talus to the fibula. There are a few talofibular ligaments such as the posterior talofibular and anterior talofibular ligament named after their relative position (Figure 10). In the foot, there are a few important ligaments such as the spring ligament and the deltoid ligament. The spring ligament attaches from the calcaneus to the navicular bone on the lateral side of the foot and has the important function of supporting the head of the talus (Figure 11). The deltoid ligament is actually a few different ligaments on the medial side of the foot that attach to the tibia and help form the ankle joint (Figure 10). Another ligament on the inferior side of the foot is the plantar fascia which helps tighten the arch of the foot from the calcaneus to the proximal phalanges (Figure 11). The plantar fascia has slightly different mechanical properties in comparison to the rest of the ligaments in the foot.

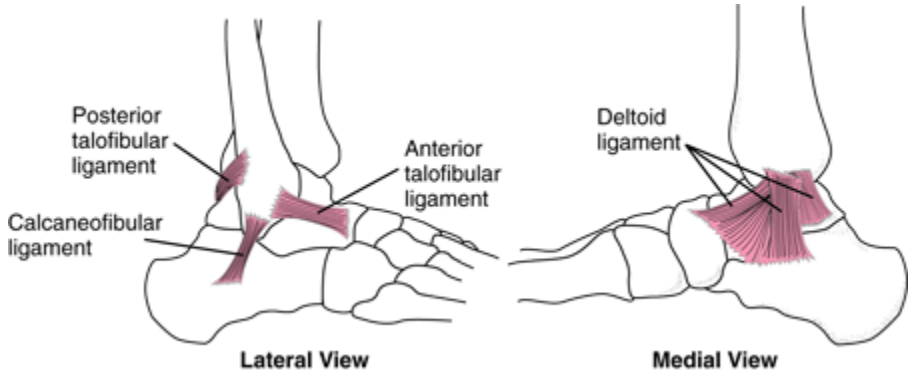

Figure 10: Diagram that shows locations of the talofibular, calcaneofibular, and deltoid ligament on lateral and medial views of the foot (Campagne, 2014)

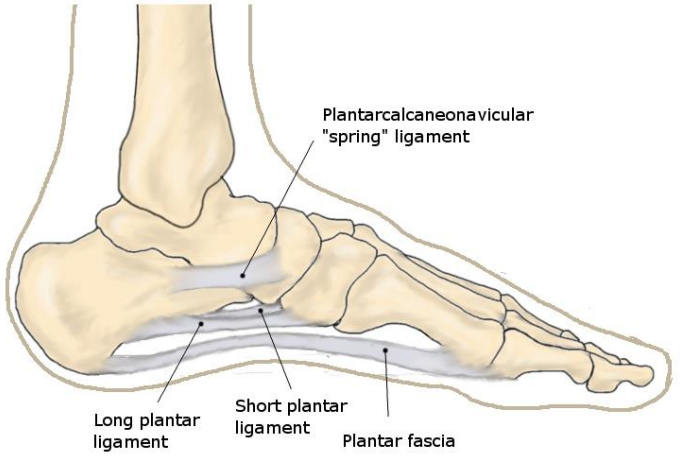

Figure 11: Diagram that shows locations of spring ligament and plantar fascia (Somastruct, 2017)

2.1.2.4. Tendons

Muscles generate force to power the motion of the bones, but they do not directly attach to bones. Tendons are the fibers that connect from bones to muscles transferring the load from one to the other. Tendons are made up of a durable and flexible material that can carry large forces. Similar to ligaments, tendons have an origin and insertion point. The origin of the tendon is located on the muscle it attaches to and the insertion is located on the bone it attaches to. Tendons are typically longer and thicker than ligaments, but their shape and size depend on their location and purpose. The most commonly known tendon in the foot is the Achilles tendon which runs from the calcaneus bone to the calf muscle (Figure 12).

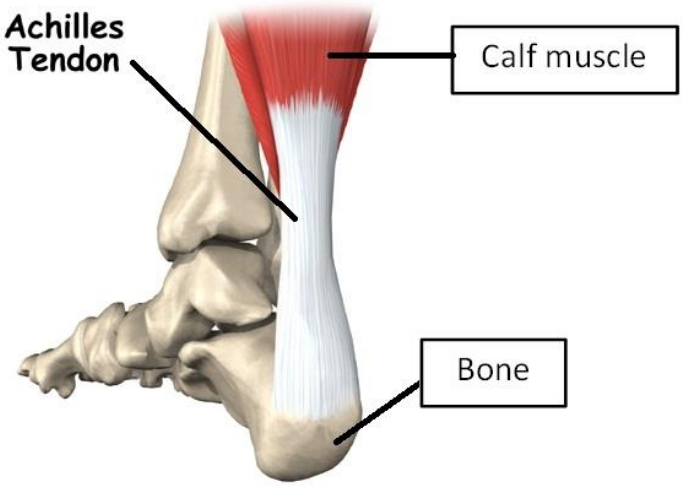

Figure 12: A posterior view of Achilles tendon attaching from the calcaneus bone to the calf muscle (Achilles Tendon Problems, 2017)

2.2. Adult Acquired Flatfoot

2.2.1. Definition

Adult-Acquired Flatfoot is an age-related degeneration of supporting ligaments that allows the arch in the foot to collapse. The spring and deltoid ligaments are responsible for maintaining the shape of the arch (Figure 13) and they are damaged over time due to aging and obesity. Flatfoot is also commonly known as posterior tibial tendon dysfunction. Elastic properties of the tendon decrease and contribute to the arch collapsing. There are four different stages of Flatfoot, and patients that reach the second stage of Flatfoot will usually seek out an orthopaedic specialist. In the second stage, patients experience pain in the medial hindfoot and will develop a flexible deformity. As the deformity becomes worse, the patient will notice that they are not able to lift their hindfoot or perform a heel rise. The third and fourth stages occur when the deformity is no longer flexible and the ankle starts to change shape.

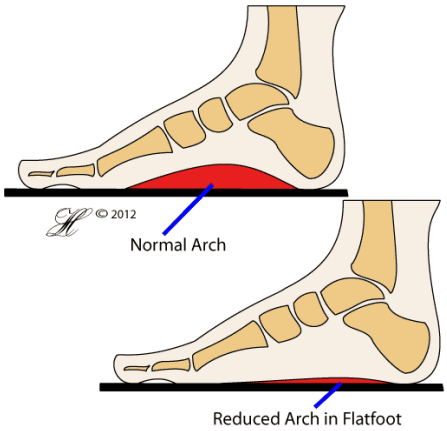

Figure 13: Diagram that shows the difference between a normal arch in a healthy foot and a reduced arch in Flatfoot (OrthoAnswer, 2012)

There are typically four physical changes which are malalignments in the foot that occur when the ligaments and tendons are attenuated. First, hindfoot valgus occurs when the hindfoot starts to move away from the body's midplane. Looking at the posterior side of the foot in Figure 14, there is an angle at the joint between the lower leg and hindfoot.

Figure 14: Hindfoot valgus represented by an angle between the lower leg and the hindfoot (Latt, 2017)

Second, midfoot planus occurs. Midfoot planus is the technical term for the arch collapsing. There is an imaginary line (Figure 15) from the center of the talus to the center of the first metatarsal head known as Meary's angle. Healthy feet will have a Meary's angle of zero degrees. Midfoot planus is defined as this angle being larger than four degrees in the convex downward position (Mudgal). The development of this angle leads to the loss of the arch in the talonavicular joint (Figure 16). As the angle gets larger, the deformity will go from mild, to moderate to severe. Definitions of mild, moderate, and severe midfoot planus deformity can be found in Table 1 below.

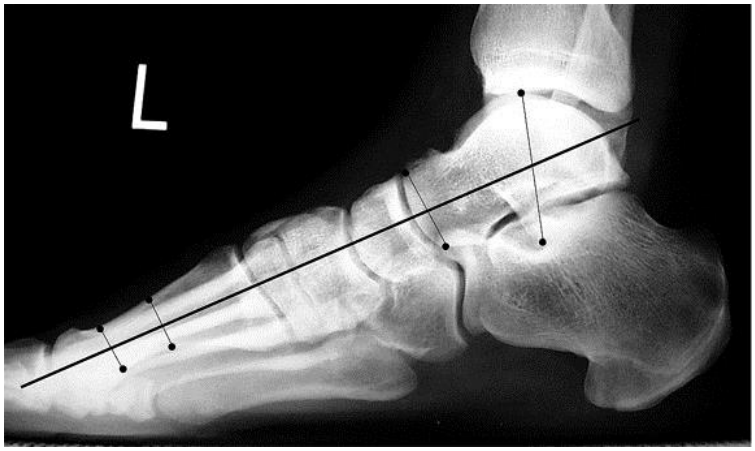

Figure 15: Imaginary line between talus and first metatarsal to define Meary's angle (Pes Cavus, 2016)

Figure 16: Midfoot planus represented by loss of arch at talonavicular joint (Latt, 2017)

Table 1: Severity of midfoot planus defined by Meary's angle value

Meary's Angle	Severity of Deformity
Angle < 15 degrees	Mild
15 degrees < Angle < 30 degrees	Moderate
Angle > 30 degrees	Severe

Third, forefoot abductus (Figure 17) is the malalignment in which the forefoot moves away from the body's midplane. Forefoot abductus is caused by the subluxation of the talonavicular joint. This condition contributes to the "too many toes" sign with Flatfoot. That sign is visible when toes can be seen on the lateral side of the foot from a posterior viewpoint.

Figure 17: Forefoot abductus represented by the subluxation of the talonavicular joint (Latt, 2017)

The fourth malalignment known as fixed forefoot supination (Figure 18) is not as common as the other three malalignments. Forefoot supination is defined as the medial side of the forefoot lifting up to roll the foot outward. This is a normal part of gait during the push-off phase, but it becomes a problem when it occurs permanently during midstance.

Figure 18: Fixed forefoot supination represented by the forefoot rolling outward (Latt, 2017)

2.2.2. Treatment

About two out of every three cases of Flatfoot are treated with nonsurgical aids. Orthotic insoles (Figure 19) and braces (Figure 20) are used to help support the arch in the foot and keep the ligaments from attenuating further. These nonsurgical devices help relieve the patients' pain symptoms.

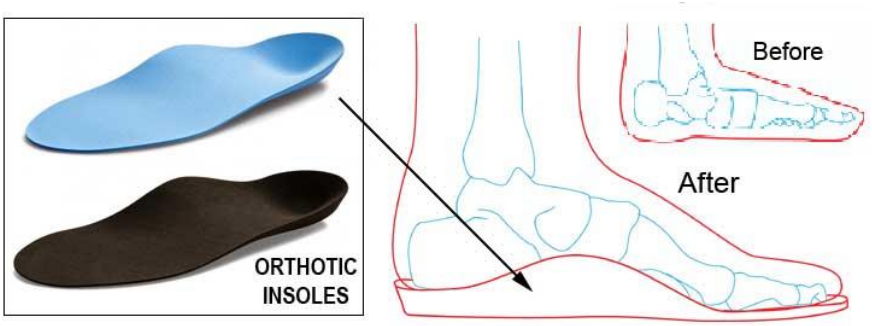

Figure 19: Example of an orthotic insole for non-operative treatment of Flatfoot (Takano, 2014)

Figure 20: Examples of foot braces for non-operative treatment of Flatfoot (Latt, 2017)

Surgical treatment is often performed by orthopaedic surgeons when patients complain of pain and interruption of their daily routine. Several different options are available to the orthopaedic surgeon such as lateral column lengthening, cotton osteotomies, heel cord lengthening, and tendon transfer.

Lateral column lengthening is a procedure during which a surgeon elongates the lateral side of the foot. The calcaneus is cut on the lateral side in order to insert a wedge that rotates the midfoot around the talar head. Wedges can either be extracted from the patient's pelvis or obtained from a company like Paragon 28 (www.paragon28.com) (Figure 21 Figure 22). Wedge sizes for lateral column lengthening usually range from 6 to 12 millimeters.

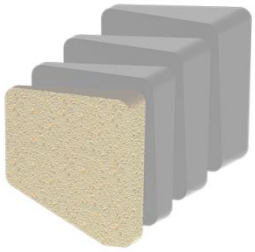

Figure 21: Paragon 28 wedges used for lateral column lengthening (Paragon 28)

Figure 22: Paragon 28 simulation of wedge implanted for lateral column lengthening using Gorilla™ HEvans™ plates (Paragon 28)

Lateral column lengthening will help correct the forefoot abduction and hindfoot valgus malalignments. The procedure can be performed in two different ways, either with a Hintermann's osteotomy or an Evans' osteotomy. The Hintermann's ostetomy cuts into the calcaneus at the sinus tarsi (Figure 23). The Evans' osteotomy cuts into the calcaneus 10 mm proximal to the calcaneocuboid joint (Figure 24).

Figure 23: Hintermann's osteotomy represented by inserting a wedge at the sinus tarsi of the calcaneus (Latt, 2017)

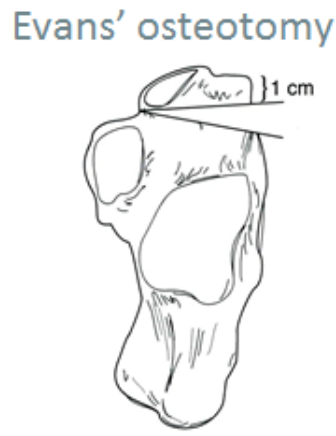

Figure 24: Evan's osteotomy represented by cutting 10 mm proximal to the calcaneocuboid joint (Latt, 2017)

A cotton osteotomy (Figure 25) is a procedure that helps push the medial forefoot to the ground. During this operation, a wedge is inserted into the superior part of the medial cuneiform. Wedge sizes for cotton osteotomies usually range from 5 to 8 millimeters. This helps correct the midfoot planus by forcefully forming an arch. This also helps correct fixed forefoot supination by forcing the distal part of the foot to ground. The cotton osteotomy is usually used to fine tune a lateral column lengthening.

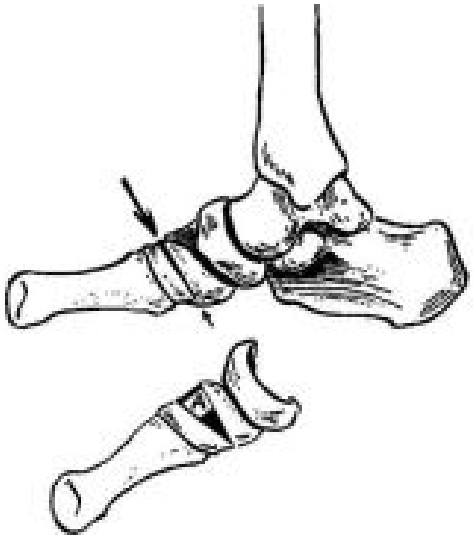

Figure 25: Cotton osteotomy represented by cutting and inserting a wedge into the medial cuneiform (Cotton, 1936)

Heel cord lengthening (Figure 26) is another procedure that can help correct midfoot planus. The operation consists of cutting the posterior section of the calcaneus and moving it down. This allows the heel cord to stretch and increases motion in the ankle joint.

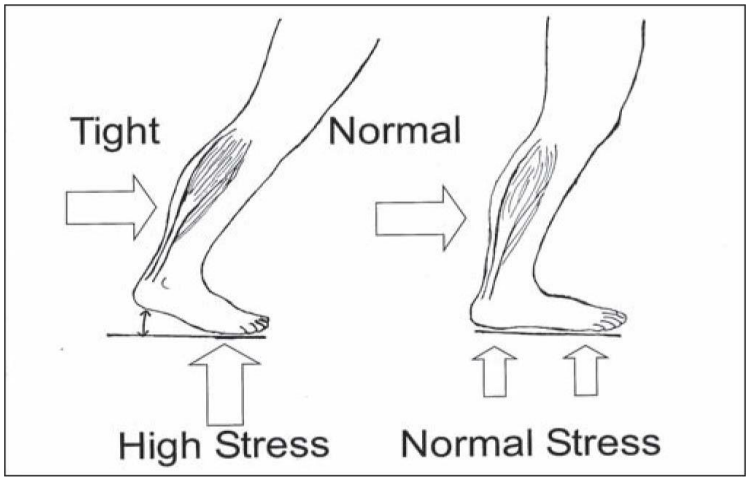

Figure 26: Diagram showing the difference in stress between a normal and tight heel cord (Laborde, 2010)

The number of surgical options available that can simultaneously correct Flatfoot malalignments is a challenge for orthopaedic surgeons. Choosing the correct options as well as the correct wedge sizes can be difficult without trial and error, but a patient should only have to endure the least number of operations to correct their problems. To make the decisions related to the minimum number of operations, a three-dimensional model of a foot will be useful for simulations prior to surgery. Different osteotomies and wedge sizes can be simulated in order to determine the contact stresses in the joints following specific surgeries.

2.3. Finite Element Method

The finite element method is a numerical method for solving partial differential equations. Detailed and complex geometries can be difficult to solve using simple equations from mechanical behavior of materials. The finite element method takes a large problem and divides it into smaller and simpler parts called finite elements. Simplifying the geometry into hexahedral or tetrahedral elements allows the use of simple mechanical equations for each element. The elements are defined by the points on the geometry known as nodes. Once the entire geometry is represented by its respective elements, the elements all together are known as the mesh (Figure 27). Finite element analysis can be used to solve several types of problems such as structural, thermal, aeroelastic, acoustic, and many more. Figure 28: Volumetric mesh of a foot represented by tetrahedral and truss elements (Cheung et al., 2005) shows how the complex geometry of a foot can be made into a mesh of smaller and simpler elements.

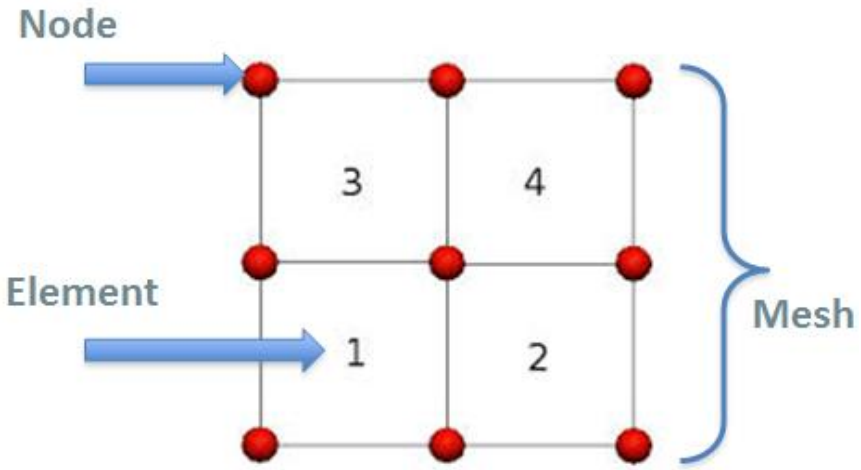

Figure 27: Diagram of a mesh created by nodes and elements

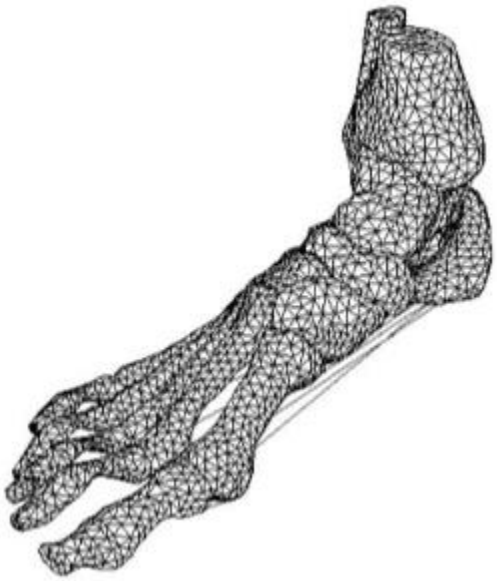

Figure 28: Volumetric mesh of a foot represented by tetrahedral and truss elements (Cheung et al., 2005)

In order to understand the basic fundamentals of the finite element method, consider a simple element such as a spring. Analysis of the force exerted by a spring requires a simple equation that relates force, stiffness, and displacement (Equation 1).

$$F = ku$$

$$F = force; k = stiffness; u = displacement$$

Equation 1: Relation between force, stiffness and displacement

A single spring element (Figure 29) has two nodes that make up the single spring element.

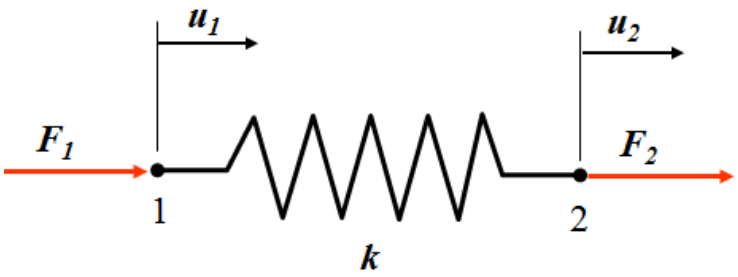

Figure 29: Linear spring element with nodes, nodal displacements, and nodal forces (Jeelani, 2015)

A spring element only has one degree of freedom, so each node can only displace in one direction. Each node also has a force in one direction. Therefore, Equation 1 can be expanded into matrix form (Equation 2). In finite element analysis, forces and materials are usually known and displacements are unknown. Equation 2) Force relation in matrix form can be rearranged to solve for the displacements in Equation 3.

$$\begin{bmatrix} F_1 \\ F_2 \end{bmatrix} = \begin{bmatrix} k & 0 \\ 0 & k \end{bmatrix} \begin{bmatrix} u_1 \\ u_2 \end{bmatrix} \; where \; F_1 = ku_1 and \; F_2 = ku_2$$

Equation 2) Force relation in matrix form

$$\begin{bmatrix} k & 0 \\ 0 & k \end{bmatrix}^{-1} \begin{bmatrix} F_1 \\ F_2 \end{bmatrix} = \begin{bmatrix} u_1 \\ u_2 \end{bmatrix} \; where \; u_1 = \frac{F_1}{k} and \; u_2 = \frac{F_2}{k}$$

Equation 3) Displacement relation in matrix form

The equations above become more elaborate as more elements, nodes, and materials are necessary in complex models.

In order to perform a finite element analysis, there are five fundamental components that must be known:

1) Geometry
2) Mesh (Finite elements)
3) Material properties
4) Boundary conditions
5) Loading

Consider the spring example in Figure 30 to understand the five fundamental components of finite element analysis. First, geometry needs to be created. In this example, the geometry is two different types of springs connected together. Second, the mesh consists of two spring elements for a total of three nodes. Both spring elements share a node in the middle. Third, each spring has a different material constant, k, so one spring will be stiffer than the other. A

fourth and important part of the finite element method includes the boundary conditions. In this example, node 1 is fixed, meaning node 1 will have zero displacement. Fifth, the loading must be specified. Node 3 is specified to have a force, P, acting away from the other nodes. From this information, equations similar to Equation 2 can be formulated to find displacements, stresses, and strains. This is the same process performed for any complex geometry such as the foot.

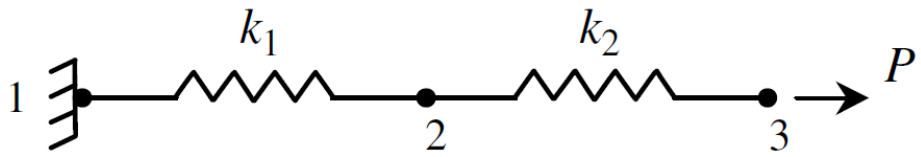

Figure 30: Spring example problem (Ashkan, 2014)

2.4. Literature Review

There are several published finite element models of the foot, but not many have been used for Flatfoot analysis. The most common applications of the finite element models of feet have been used for diabetes research (Cheung et al., 2004), shoe design (Cheung, et al., 2005), and gait analysis (Chen et al., 2001; see also Chen et al., Sep. 2014). The only journal article describing a finite element model for Flatfoot analysis was about the model itself (Wang, 2014). That model can be seen in Figure 31. There were no publications describing ways to improve surgical planning for this condition with mathematical methodology. Therefore, there is a demand for scientific studies of Flatfoot analysis with the finite element method.

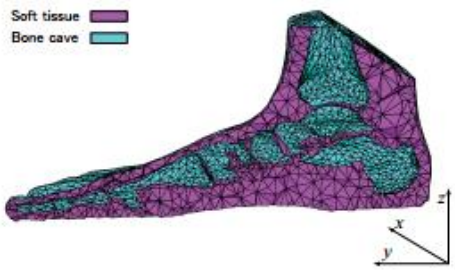

Figure 31: Cross-section view of volumetric mesh from Pes Planus study showing elements representing bone and soft tissue (Wang, 2014)

Examining finite element models in published articles showed that all models had simplified the geometries they were modeling. The bones were usually modeled from medical images which made the shapes anatomically correct, but the materials properties of different bones and different regions of specific bones were not accounted for. There was no difference in cortical or trabecular bone structure or properties. They had used a blended bone property that involved

an average of the bone material properties (Crowninshield & Nakamura, 1981). Also, the ligaments and tendons were only modeled as truss elements that can only have one cross-sectional area (Figure 32). Ligaments and tendons usually have varying cross-sectional areas along their length from the origin to insertion point.

Figure 32: Volumetric foot mesh with ligaments modeled as truss elements (Spyrou, 2011)

Structures like the spring ligament, deltoid ligament, posterior tibial tendon, and Achilles tendon have a significant impact on how Adult Acquired Flatfoot deforms the foot and how it can be corrected. Therefore, the finite element model should represent the varying cross-sectional areas and complicated load paths of ligaments and tendons to give the most realistic simulation. With the objective to find the most realistic results, the goal of this study was to create an anatomically and physiologically correct finite element model of the foot and ankle for Flatfoot analysis.

3. FINITE ELEMENT METHOD

3.1. Geometry

3.1.1. Bone Assembly

3.1.1.1. CT Scan Collection of a Cadaver Foot

Medical images of a human foot were used to develop the most realistic bone geometry possible. In order to get the best quality images that show the difference in cortical and trabecular bone, computed tomography (CT) was used. A CT scan takes several images of an object by taking cross-sectional images from different angles. Images are gathered from a CT machine in the three anatomical planes: coronal, sagittal, and axial directions (Figure 33). This type of imaging exposes patients to radiation, so a cadaver was used in order to gather images of a human foot. The cadaver was chosen based on its age and availability. The age of the cadaver (50 years old) best matched the age of patients that normally develop Flatfoot (Chimenti, 2014). The cadaveric limb from this cadaver had not previously been used for mechanical testing reducing the risk that it had been damaged prior to scanning. The scanned specimen was a foot sectioned at the tibia and fibula several inches superior to the ankle joint. Therefore, images were taken of the entire cadaver specimen. A CT scanner from the Banner University Medical Center in Tucson, Arizona was used to scan the images. The CT scanner's make and model were unknown. To receive the most precise anatomical data, the scanner was set to gather images at the thinnest slice separation, which was 0.6 millimeters.

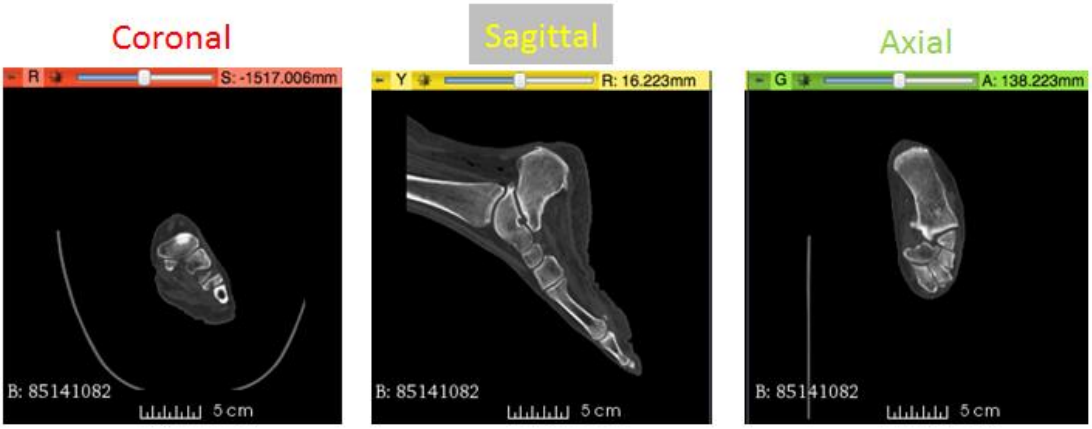

Figure 33: Coronal, sagittal, and axial cross-sectional CT images of the scanned specimen in 3D Slicer

3.1.1.2. 3D Representation of the Foot and Ankle Bones

After gathering images from three anatomical planes of a cadaver foot, the two-dimensional images were stitched together to create three-dimensional geometry. Although one of the best software programs for this is Mimics, (Materialise, http://www.materialise.com/) the software program cost was beyond our budget and a different software program 3D slicer

(https://www.slicer.org/) was selected. 3D Slicer is a freeware open-source medical image processing and visualization software tool. The cost, accessibility, and user interface made it the best option at the time to translate two-dimensional images to three-dimensional geometry representations.

After downloading version 4.4.0 of 3D Slicer, CT scanned images were loaded into the program. In order to focus attention on each bone's complex details, each bone was isolated. Images from each anatomical plane were cropped by setting boundaries around each individual bone. Pixel intensity threshold ranges were automatically set to identify bone tissue (Figure 34). In order to separate cortical from trabecular bone, threshold values were manually changed to isolate cortical bone. After receiving a rough outline of the cortical bone shell, each cross-section from each anatomical plane was examined. Each cross-section needed to correctly isolate only the cortical shell of each specific bone. Thresholds were manually changed to remove tissues that should not have been included and to fill in areas that needed to be included. Changes made in one cross-section affected other cross-sections. Therefore, each cross-section was checked a second time to ensure no holes or gaps were created. After a second observation of all the cross-sections for one bone, a three-dimensional representation was made for the cortical bone (Figure 35).

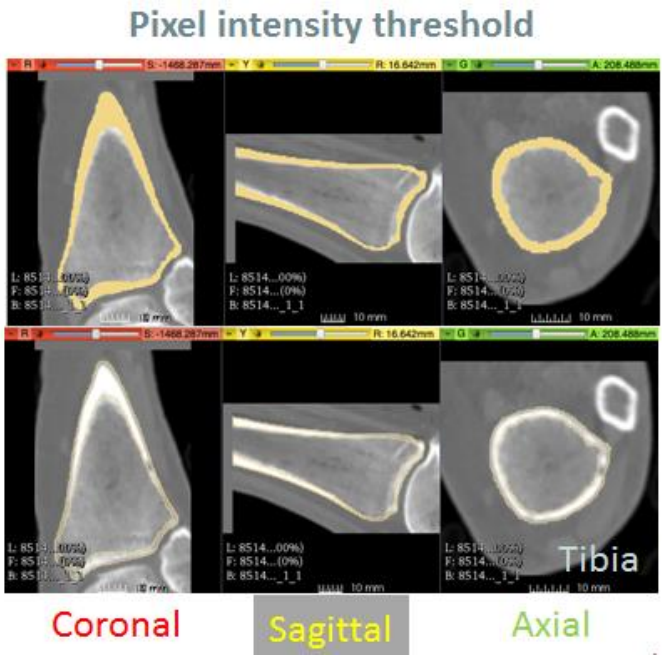

Figure 34: Cortical bone identified by pixel intensity threshold using 3D Slicer

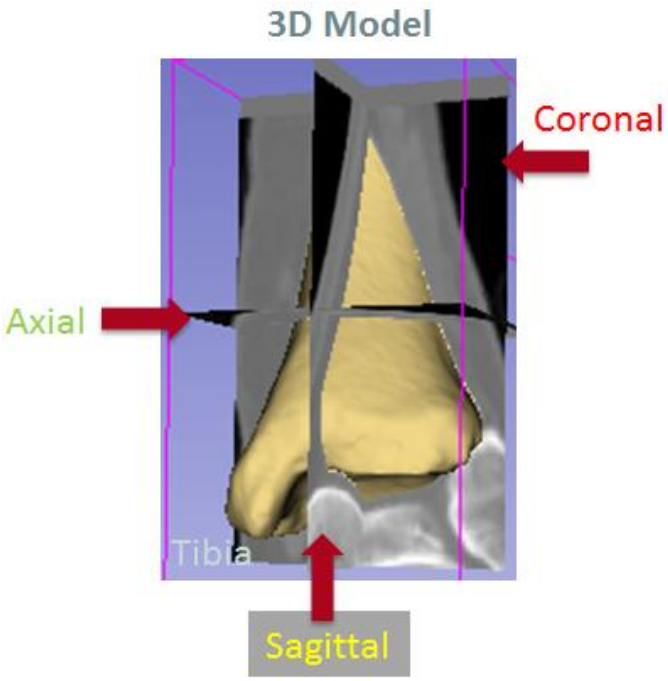

Figure 35: 3D model of cortical bone of tibia created from assembling 2D cross-sectional images in 3D Slicer

The processes described were performed for each individual bone's cortical shell. The solid representations of the 1st metatarsal, calcaneus, and multiple bones of the foot can be seen in Figures Figure 36,Figure 37, andFigure 38 respectively. Instead of performing this vigorous process for the trabecular bone of every bone, a different software program called SolidWorks (Dassault Systemes, http://www.solidworks.com/) was used to easily fill in the cortical shells. This not only saved time, but ensured that the faces of the cortical and trabecular bone surfaces met at the same location.

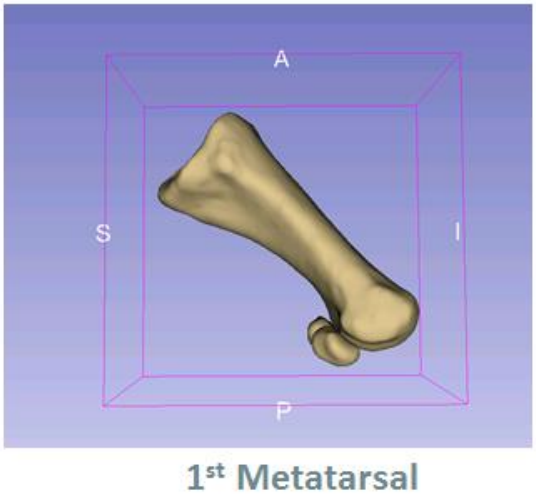

Figure 36: 1st metatarsal cortical bone model in 3D Slicer

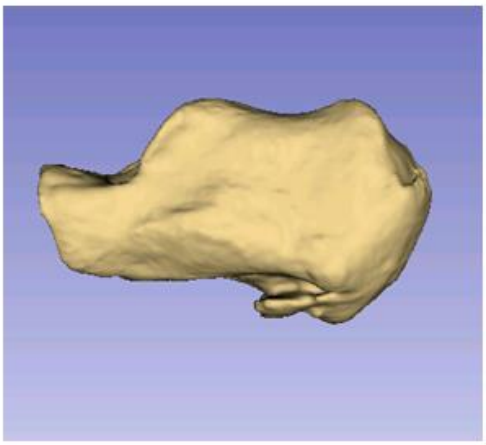

Figure 37: Calcaneus cortical bone model in 3D Slicer

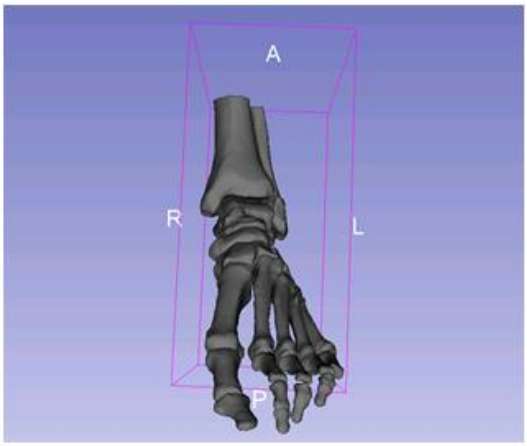

Figure 38: Multiple cortical bone models of the foot in 3D Slicer

3.1.1.3. Reduction of Surface Geometry

SolidWorks has a limit on the number of faces that can be imported. The representation of each bone from 3D Slicer was made up of thousands of miniscule triangles to account for all the complex details of the geometry. The large number of triangles had to be reduced in order to be to import them into SolidWorks. A software program called 3-matic (Materialise, http://www.materialise.com/) was used to reduce the surface geometry. A procedure from a dissertation (Bernal Covarrubias 2015) was used to reduce the number of triangles that made up the surface of each bone. Triangle reduction was completed using tools that evaluated height/base ratios, maximum edge lengths, and geometrical error.

Figure 39 shows the reduction in surface geometry using 3-matic for the tibia bone. Figure 40 shows that by overlapping the original and reduced surface geometry, there are no

overwhelming discrepancies between the two geometries. Focusing on a small sectioned area of the overlapping geometries, there is a significant amount of reduction in the surface geometry without losing much detail.

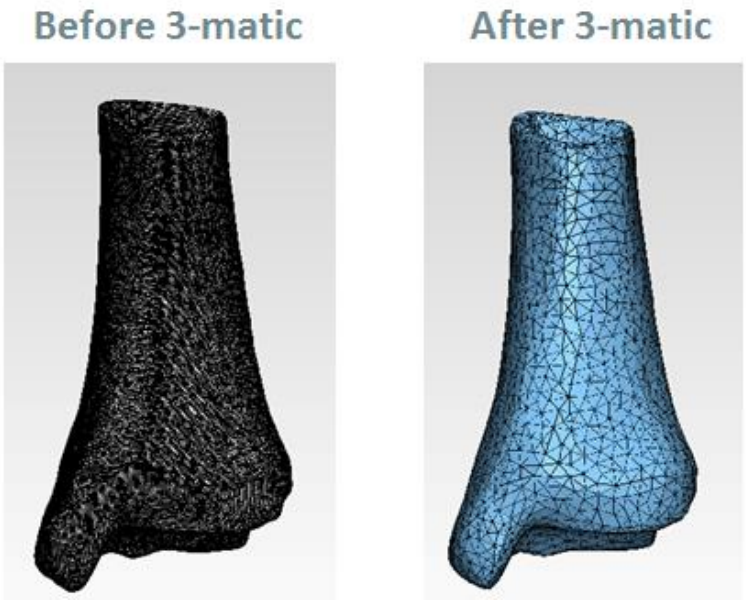

Figure 39: Surface mesh of tibia cortical bone before (left) and after (right) using 3-matic

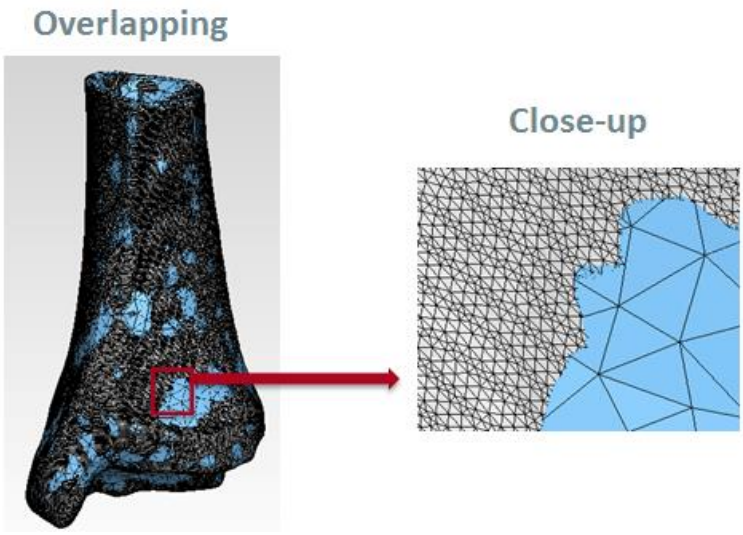

Figure 40: Surfaces meshes of tibia cortical bone overlapped to show no overwhelming discrepancies between models before and after 3-matic

3.1.1.4. Assembly of Cortical and Trabecular Bone

After the surface geometry was reduced for each bone, each bone was successfully imported into SolidWorks. In order to make the trabecular bone, each cortical bone shell was filled in

using a feature in SolidWorks. By selecting the inner surface of the cortical shell and using the Filled Surface tool, a trabecular body was made that shares the same face of the cortical shell (Figure 41).

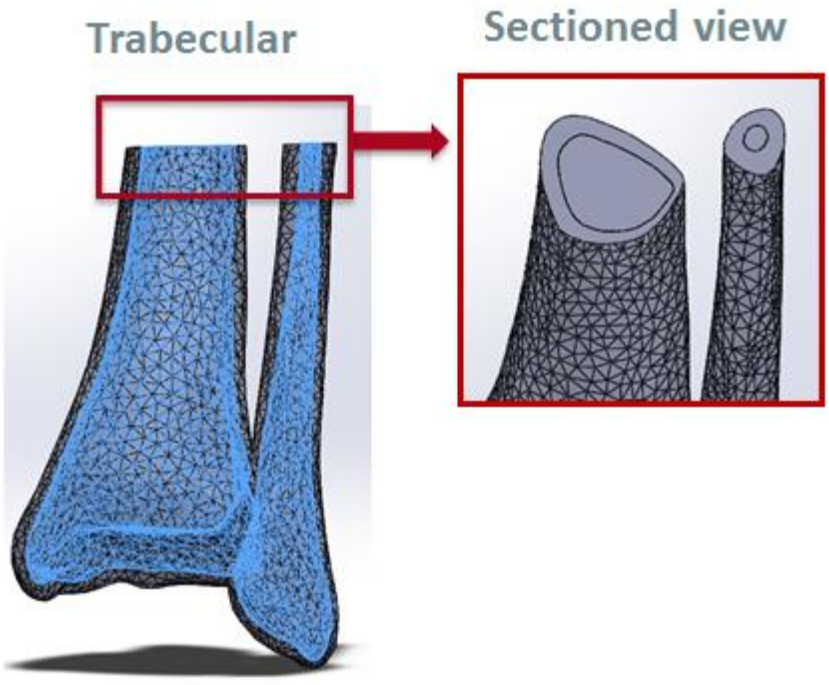

Figure 41: Tibia trabecular bone represented in blue color on left; sectioned view of trabecular bone within cortical bone on right in SolidWorks

After importing all bones with their trabecular and cortical bodies into one assembly, the tibia and fibula were noted to be at the wrong angle i.e. they were not at a 90 degree angle with respect to the ground (Figure 42). This angle is important in order to best simulate the foot in the midstance position which is 90 degrees. First, a ground plane was created from three specific points: the most superior points of the calcaneus, first metatarsal head, and fifth metatarsal head. After creating the ground plane, a line was created from the center of mass of the talus bone to the center of the mass of the second metatarsal. The tibia and fibula were then rotated parallel to this line around the center of mass of the talus bone until the tibia and fibula were perpendicular to the plane of the ground.

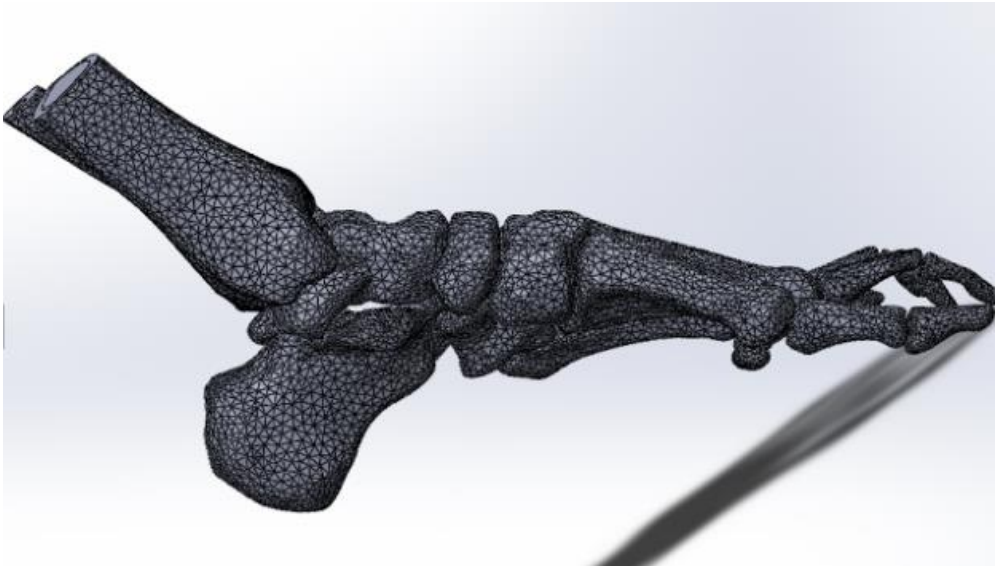

Figure 42: Foot bone model before rotating tibia and fibula in SolidWorks

After rotating the tibia and fibula, the superior part of these two bones were sectioned in a way that made them parallel with the ground plane. The final bone assembly including the rotated tibia and fibula can be seen in Figure 43. The left image outlines the surface geometry of each bone and the right image is the same as the left without the surface geometry outlined.

Figure 43: Final foot bone assembly in SolidWorks

3.1.2. Cartilage Assembly

After developing the bone geometry, the cartilage was modeled. Cartilage and similar internal tissues are not represented well in CT scans, so the cartilage was modeled manually in SolidWorks. As stated before, cartilage belongs on any part of bone expected to articulate with other bones. Following alongside an interactive resource (Figure 44), surfaces of the bones were extruded to represent the cartilage. The cartilages of each bone meeting in joint movement would have a relatively similar thickness. That thickness was determined as the largest thickness before the cartilage surfaces would penetrate one another. Thicknesses ranged from 0.1 to 1 millimeter. The final cartilage assembly and a zoomed-in section can be seen in Figure 45.

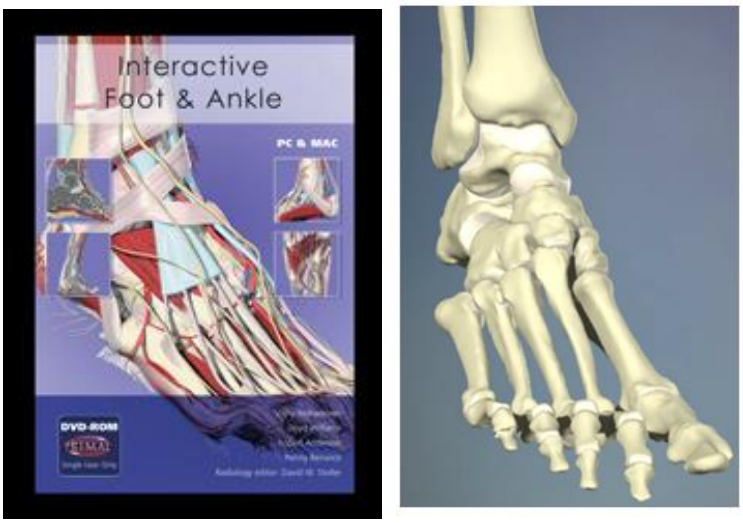

Figure 44: Online resource (Interactive Foot & Ankle) used to create cartilage, ligaments, and tendons (Mahadevan)

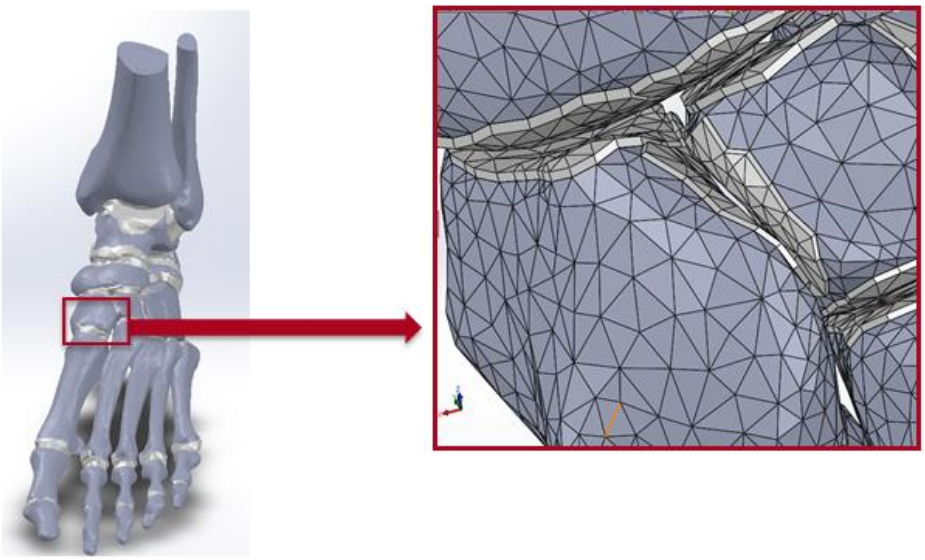

Figure 45: Cartilage extrusions (represented in white color) created where bone is expected to articulate made in SolidWorks

3.1.3. Ligament and Tendon Assembly

Ligaments and tendons are also not represented well in CT scans. Therefore, the ligaments and tendons were also modeled manually in SolidWorks. The foot has hundreds of ligaments and tendons, so an orthopaedic surgeon provided guidance on which were important to simulate in the model. Then, the origins, insertions, and cross-sectional areas of the ligaments and tendons were included in the model. Textbooks of human anatomy and published journal articles were used to find most unknown quantities (Netter & Colacino, 1997; see also Boss & Hintermann, 2002; Campbell et al., Apr. 2014; Golanó et al., 2010). The online resource that helped modeling cartilage was then used to estimate the rest (Mahadevan). An example of a resource can be seen in Figure 46. The final geometry of the ligaments and tendons were examined and approved by the orthopaedic surgeon supervising this study.

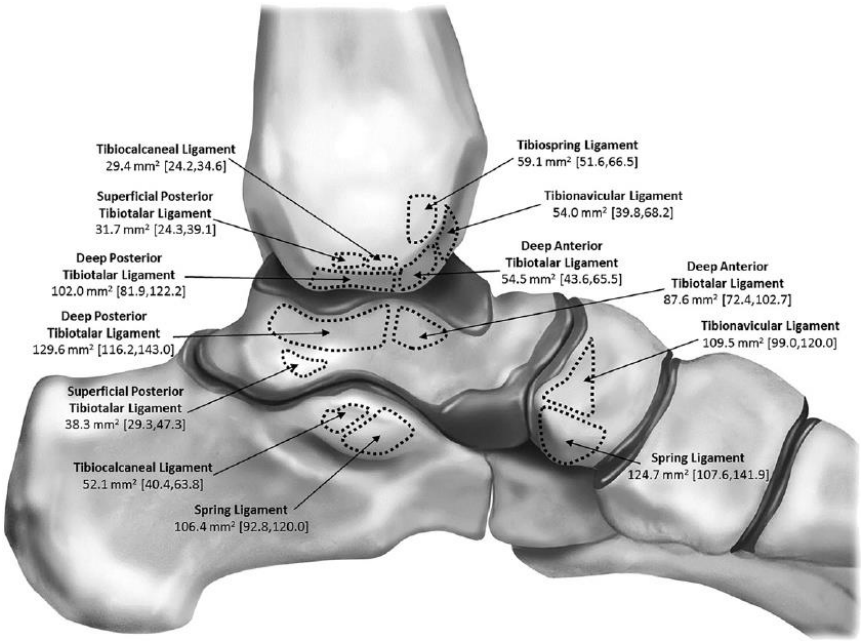

Figure 46: Cross-sectional areas and locations of ligaments on the medial side of the foot (Campbell et al., 2014)

All ligaments had their origins and insertions located on an external surface of a bone. Tendons also had their origins located on the external surfaces of bones, but the insertions are technically on muscles not being modeled. Therefore, all tendons had their insertion points at the cross-section of the superior portion of the tibia and fibula. Modeled ligaments can be seen in Figure 47 as the red colored bodies. Modeled tendons can be seen in Figure 48 as the white colored bodies.

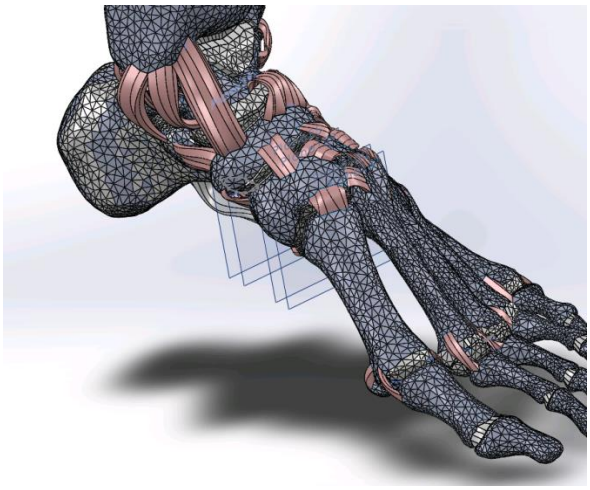

Figure 47: Ligaments (represented in red color) assembled in SolidWorks

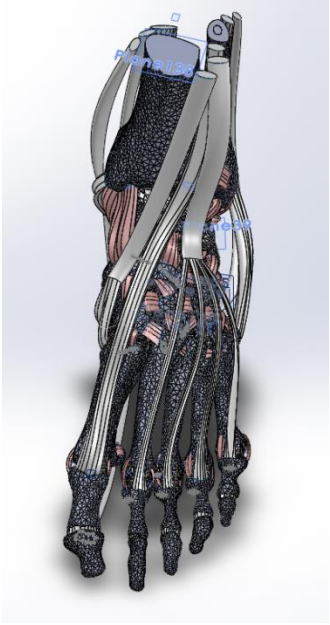

Figure 48: Tendons (represented in white color) assembled in SolidWorks

3.1.4. Ground Surface

A ground surface was created in order to interact with the inferior bones of the foot. A simple rectangular prism was created from the ground plane of the most inferior points of the calcaneus, first metatarsal head, and fifth metatarsal head. The thickness of the ground was set to 10 millimeters to create a thickness similar to a mat on the ground.

3.1.5. Geometry Summary

Geometry for bones, cartilage, ligaments, and tendons were created using several software programs. Bone was modeled as anatomically correctly as possible from CT scans. Cortical and trabecular bone were made into separate bodies for 24 separate bones in the foot (see Appendix A). Over 155 cartilage layers were modeled in between bones that were expected to articulate. Thicknesses of these layers ranged from 0.1 to 1 millimeter. Ligaments and tendons were also manually modeled based on origins, insertions, and cross-sections found in the literature. A total of 69 ligaments (Appendix B) and 9 tendons (Appendix C) were included in the model. Finally, a ground surface was included at the most inferior part of the foot. A final image of the geometry can be seen in Figure 49 with each part in a different color. The same image of the geometry can be seen in Figure 50 colored according to material type. These images and most of the remaining images are used courtesy of ANSYS (http://www.ansys.com/).

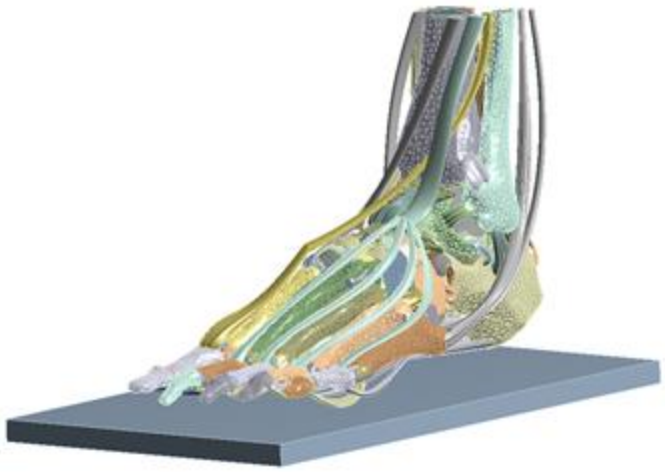

Figure 49: Foot geometry imported into ANSYS Workbench (each color represents an independent solid body)

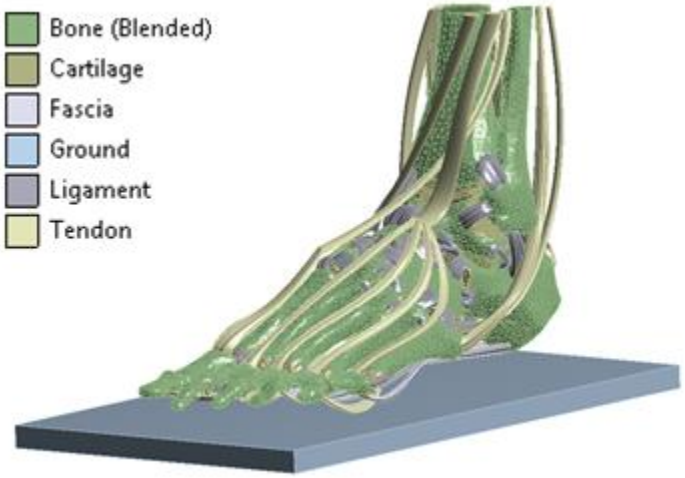

Figure 50: Foot geometry imported into ANSYS Workbench (colored by type of material)

3.2. Mesh (Finite elements)

3.2.1. Solid Elements

All foot components were represented as solid tetrahedron elements. Using default settings, ANSYS Workbench uses SOLID187 elements (Figure 51) which are three-dimensional, 10-noded elements used most commonly for complex geometries (ANSYS 17.0). The 10 nodes are made up of corner and midside nodes in order to create a bilinear or quadratic element. Quadratic elements usually yield more accurate results (ANSYS 17.0). The midside nodes allow the edges to deform, decreasing the high stiffness that linear tetrahedral elements typically experience. Each node of the tetrahedral element is only allowed to translate in the x, y, and z directions.

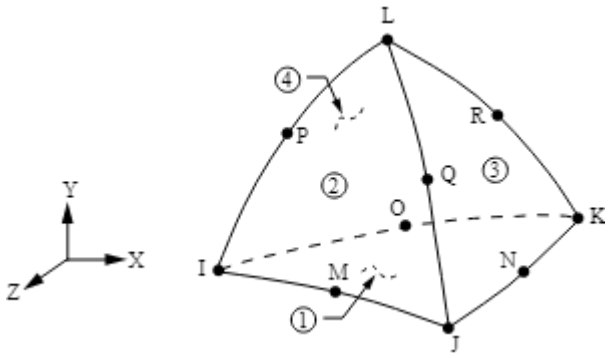

Figure 51: SOLID187 element (ANSYS 17.0)

Most research studies have modeled the ligaments and tendons as truss elements. The truss elements used most often in ANSYS are called LINK180 elements (Figure 52). LINK180 elements are three-dimensional, two-noded elements that are used for supporting tension-only and compression-only purposes of structures like trusses, cables, links, and springs (ANSYS 17.0). To support the goal of keeping the model as realistic as possible, these elements were not chosen for this simulation. Linear elements like the LINK180 are not able to simulate the curvature and bending that ligaments and tendons experience. LINK180 elements can only have one thickness, but the varying thickness of ligaments and tendons can affect the mechanical properties of the foot. Therefore, SOLID187 elements were used to represent ligament and tendons in order to incorporate the true curvature and thickness of these tissues.

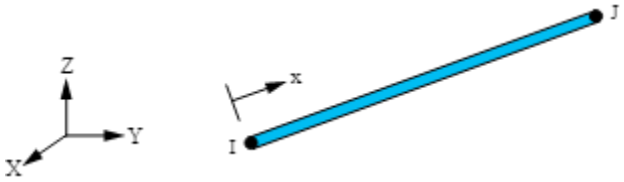

Figure 52: LINK180 element represented by nodes I and J (ANSYS 17.0)

The simple geometry of the ground support allows the usage of hexahedral or brick elements. SOLID95 elements are three-dimensional, 20-noded brick elements used in this ANSYS simulation (Figure 53). The midside nodes of the higher order elements allow for higher accuracy of curved deflection. Brick elements are less stiff than tetrahedral elements, contributing to a more accurate stress than the tetrahedral elements. The larger shape and higher accuracy of these elements decrease the total number of elements in the model. Fewer elements lead to faster solve times.

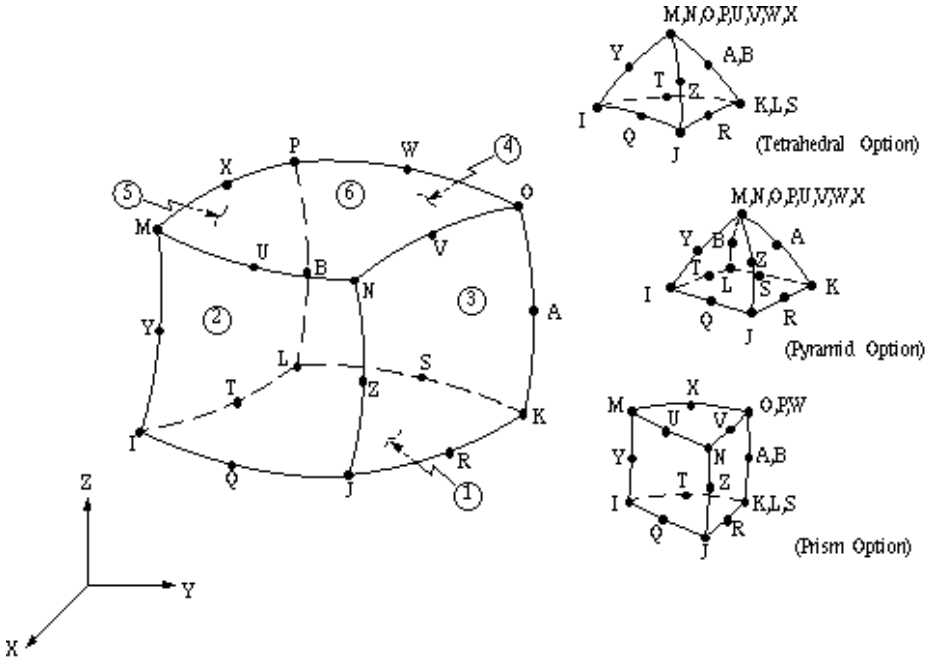

Figure 53: SOLID95 element (ANSYS 17.0)

3.2.2. Contact Elements

After meshing all volumes with solid elements, contact and target elements were added between any two surfaces that share a contact. This simulation used CONTA174 (Figure 54) and TARGE170 elements (Figure 55) for contact and target elements, respectively. CONTA174 elements are three-dimensional, 8-noded elements that can be used for surfaces with both rectangular and triangular elements on the surface (ANSYS 17.0). TARGE170 elements are created to pair with the corresponding contact elements. The contact and target elements are determined to be in contact when the contact element penetrates the target element. ANSYS uses integration points to determine the location of penetration (Figure 56). The distance between contact and target elements for the two surfaces to be in contact can be manually set, but this simulation used the program-controlled settings. Each body was examined for possible contact areas to determine a total of 650 contacts in the model. After determining the surface pairs in contact with one another, the type of contact was determined based on bodies to which surfaces belonged. Ideally, this model contains two types of contacts: bonded and frictionless contacts.

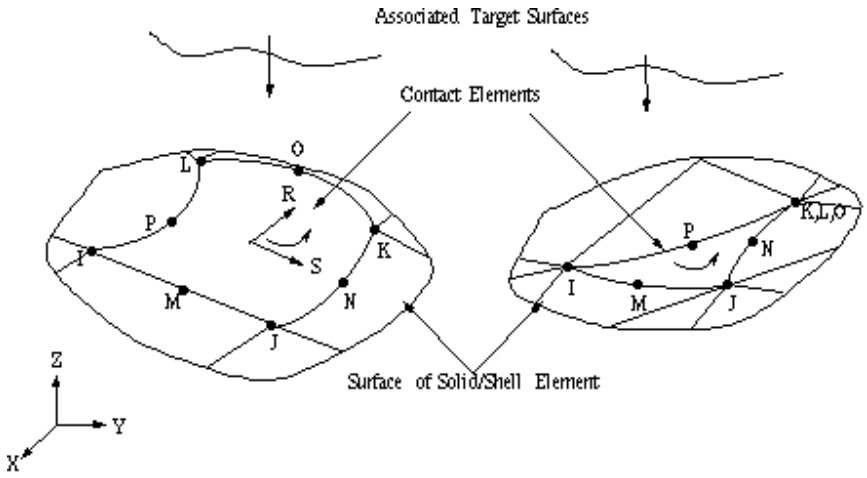

Figure 54: CONTA174 elements (ANSYS 17.0)

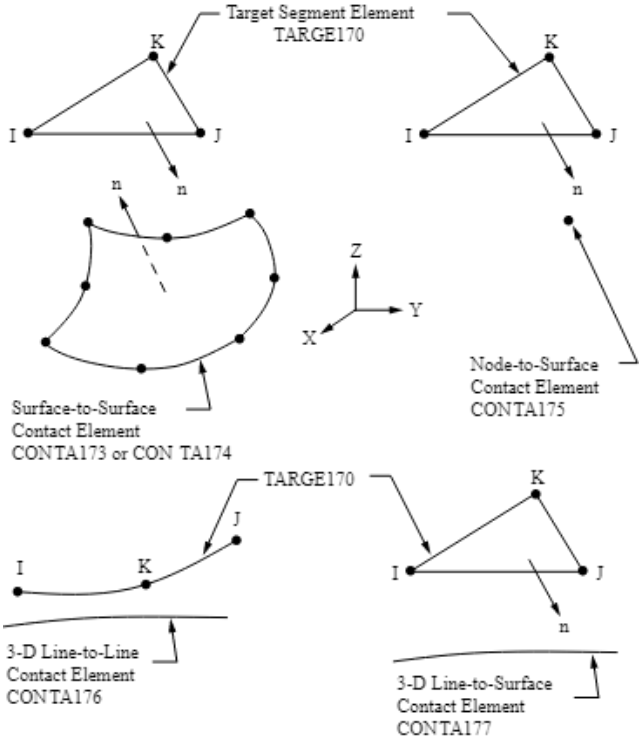

Figure 55: TARGE170 Elements (ANSYS 17.0)

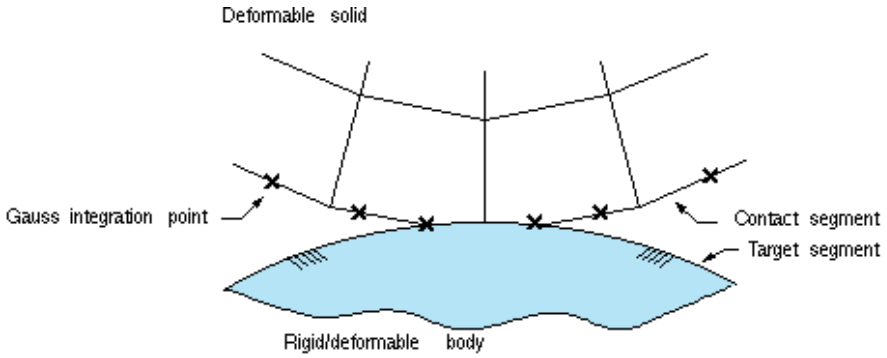

Figure 56: Contact detection using integration points to detect penetration according to ANSYS 17.0 documentation

Bonded contacts are made between two surfaces that are best described as being glued together. There is no penetration, separation, or sliding between the chosen faces and edges. In this simulation, all contact with bones was considered to have a bonded contact. The cortical and trabecular bone bodies were bonded together assuming the trabecular body would remain inside the cortical body. Cartilage sitting on a bone would remain on the bone under all circumstances. Origin and insertion areas of ligaments were also bonded to the bone. The bone-to-tendon areas were also bonded. Bonded contacts are the simplest to simulate because they are linear. Linear contacts do not rely on previous node locations or nodal deformations because the nodes in contact are always bonded together. About two-thirds of the total contacts were determined to be bonded contacts.

Frictionless contacts are made when two surfaces are allowed to slide and separate without any resistance. The best example to describe frictionless contacts is visualizing a body sliding on ice. There is no penetration between the body and the ice, but the body is not restricted from moving along the ice. In the human body, the contact between one cartilage surface and another cartilage surface is best defined as a frictionless contact. All parts made of fibrous tissue were assumed to have a frictionless contact with any other fibrous tissue. Therefore, if any ligaments and tendons could have any interaction with other ligaments, tendons, and cartilage in the simulation, a frictionless contact was made between the two surfaces. Unlike the bonded contacts, frictionless contacts are nonlinear. The current node location and nodal deformation of a nonlinear contact depends on previous iterations. In other words, a simulation with nonlinear contact needs to know the previous position of nodes in order to determine the next position. Nonlinear contacts not only significantly increase the solve time, but the system of equations become more difficult to converge to a solution. The remaining one-third of the contacts in the model was determined to be frictionless.

3.2.3. Mesh Summary

At the end of volume meshing, the final count was about 705,000 nodes and 339,000 elements. This count was made up of solid tetrahedral elements to build the foot and solid brick elements to create the ground support. Over 650 contacts were added between the bodies in the model

to create an additional 285,000 elements. In order to get initial results, all contacts were set as bonded to keep a linear system of equations, except for one contact pair. The calcaneocuboid joint was set to be frictionless in order to see preliminary results of the nonlinear contact. The final number of nodes and elements was appropriate for the accuracy necessary for a shorter run time. The shorter run times helped with troubleshooting the complex model with the nonlinear contacts.

3.3. Material Properties

Linear elastic isotropic material properties were used for all materials to keep the model simple. The material properties necessary for linear elastic materials are Young's modulus, and Poisson's ratio (Table 2). The material properties of bone were based on a blend of cortical and trabecular bone together in order to compare results with other research studies. Ligaments, tendons, and cartilage were referenced from other research simulations (Cheung et al., 2004; see also Qiu et al., Dec. 2011; Ozen et al., 2013; Maganaris & Paul, 1999; Peltonen et al., 2010). The plantar fascia is a structure similar to ligaments, but has a slightly higher Young's modulus than ligaments. The ground support had a large enough Young's modulus to be stronger than all other components, but still experience some deflection.

Table 2: Material properties of model components

Component	Density [kg/m^3]	Young's modulus [MPa]	Poisson's ratio
Bone	449	7,300	0.3
Cartilage	1000	1	0.4
Ligament	1000	260	0.4
Tendon	1000	1,500	0.4
Plantar Fascia	1000	350	0.4
Ground Support	1000	17,000	0.1

3.4. Boundary Conditions

The boundary conditions for the simulation included fixing degrees of freedom of specific components. First, the inferior face of the ground support was fixed in all three translations. Fixing the ground support in the location seen in Figure 57 keeps the ground in place without hindering deformation from contact with the inferior surface of the foot.

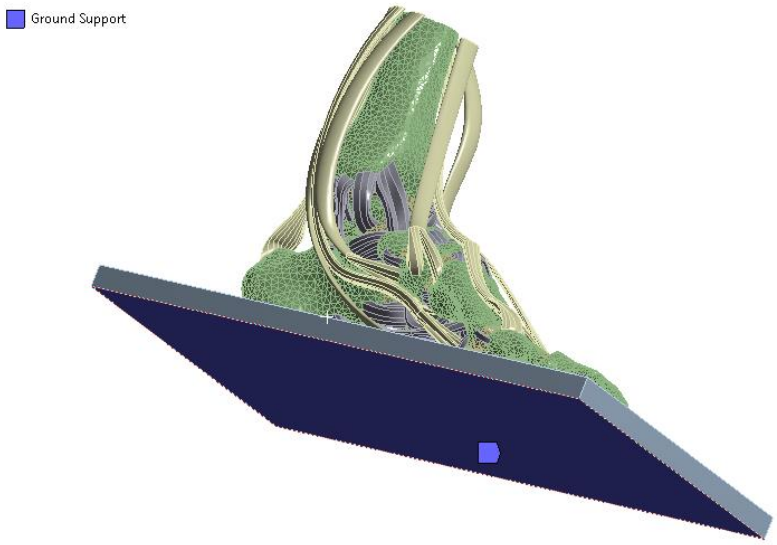

Figure 57: Bottom surface of ground support fixed in all translation in ANSYS Workbench

Next, the nodes of the phalanx bones were also fixed in all three translations (Figure 58). Fixing the nodes of the toes gave the remaining bodies of the foot an anchor point to observe relative motion. After applying loading, this boundary condition keeps the foot grounded, so there is no unusually large deformation.

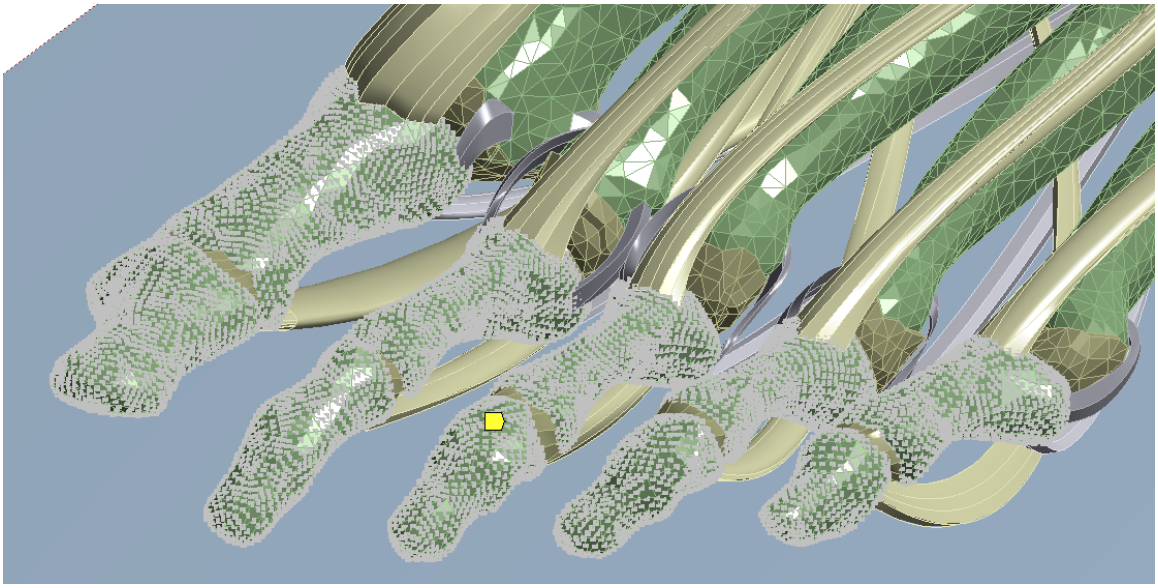

Figure 58: Nodes (represented by gray points) of toe bones fixed in all translations in ANSYS Workbench

Lastly, the superior cross-sectional areas of the tendons were fixed to keep them from experiencing unusually large deformation. Not all degrees of freedom were fixed for the tendon

cross-sections in order to allow the tendons to move in the axial direction. To only allow axial movement, a coordinate system was created at the superior cross-section of the foot. The Z direction points toward the medial side of the foot. The X direction points toward the anterior part of the foot. The Y direction points toward the superior part of the foot and also represents the axial direction of the tendons. Referencing this coordinate system, seen in Figure 59 Figure 60, the superior cross-sectional areas in the XZ plane were fixed in the X and Z direction. This left the Y (or axial) direction free to move. In Figure 59 Figure 60, the yellow areas represent the cross-sectional areas of the tendons fixed in the X and Z direction. Table 3: Cross-section labels of tendons from explains the labels of tendons in Figure 59Figure 60.

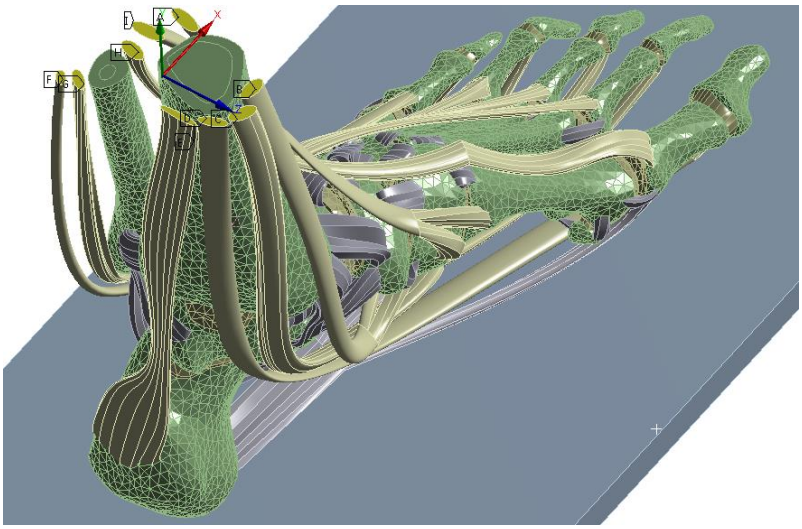

Figure 59: Superior axial cross-sections of tendons (represented in yellow color) in ANSYS Workbench

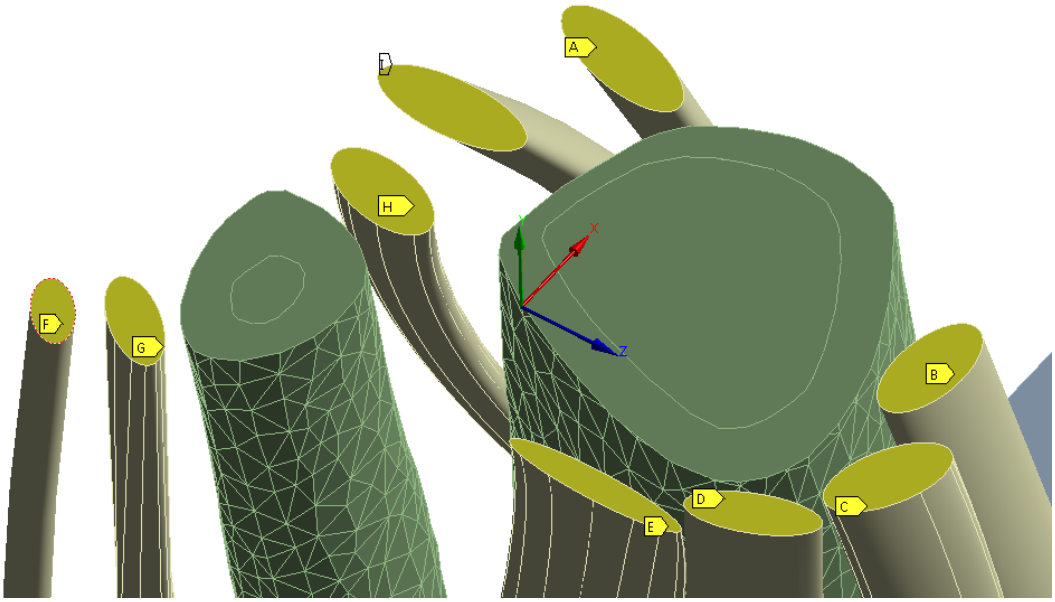

Figure 60: Close-up of tendon axial cross-sections (represented in yellow color) in ANSYS Workbench

Table 3: Cross-section labels of tendons from Figure 59 Figure 60

Designated Letter in Figure 60	Tendon
A	Anterior tibialis
B	Posterior tibialis
C	Flexor digitorum longus
D	Flexor hallucis longus
E	Achilles
F	Peroneus longus
G	Peroneus brevis
H	Extensor hallucis longus
I	Extensor digitorum longus

3.5. Loading

The loading of the simulation was based on loading of a foot in the midstance position. The two sets of forces in the model include body weight and the forces due to the muscles holding the foot in position during midstance.

The body weight of the cadaver used for this simulation was unknown. In order to compare results with a previous study (Wang et al. 2014), a body weight of 607.6 Newtons was used in the simulation. All the body weight was assumed to be acting on one foot during gait. Another assumption was that the body weight is primarily carried by the tibia. Therefore, a force of 607.6 Newtons was applied to the superior cross-sectional area of the tibia bone in the negative Y

direction of the coordinate system described in section 3.4. Figure 61: Axial cross-section shows the location and coordinate system the load is applied.

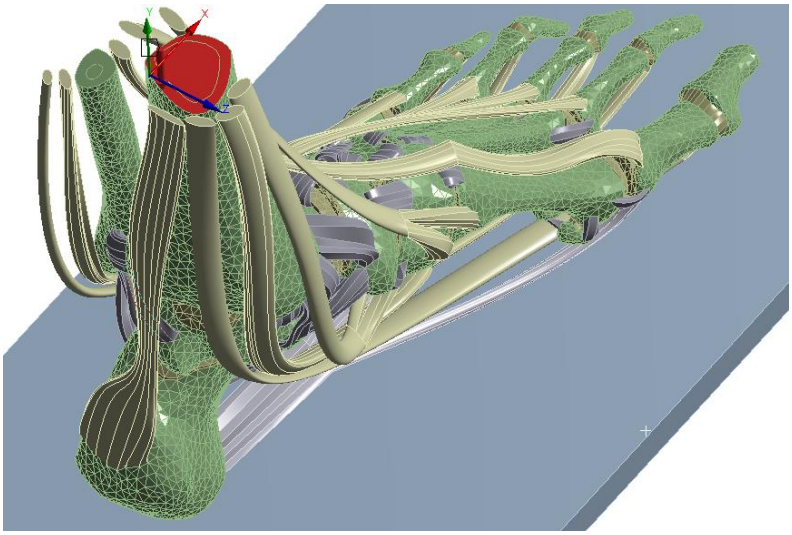

Figure 61: Axial cross-section of tibia to apply force of body weight in ANSYS Workbench

Muscle forces to hold the foot in midstance were represented as tendon forces. The magnitudes of the force for each tendon was determined from published results (Arangio & Salathe, 2002; see also Wang et al., 2014) based on body weight. The values of the forces from this calculation are summarized in Table 4. Using these calculations, the Achilles tendon carries the largest load in the foot with a magnitude of 132.53 Newtons.

Table 4: Tendon forces calculated at midstance and applied to model

Tendon	Force [N]
Achilles	132.53
Posterior tibialis	26.68
Anterior tibialis	0
Peroneus longus	21.35
Peroneus brevis	10.67
Flexor hallucis longus	13.34
Flexor digitorum longus	6.67
Extensor hallucis longus	13.34
Extensor digitorum longus	6.67

One simulation was performed in order to see how the model interacts with some nonlinear contact included in the model. This simulation has all contacts in the foot bonded together except for the calcaneocuboid joint (Figure 62). The cartilage face located on the cuboid bone in contact with the cartilage face located on the calcaneus bone was set as a frictionless contact. Changing one contact to be frictionless causes the problem to be nonlinear. In order to apply the nonlinear contact to the simulation, the simulation was separated into two load steps. In the

first load step, no forces were applied to allow the contacts to close any gaps between contact pairs. In the second load step, the body force and tendon forces from Table 4 were applied to the foot.

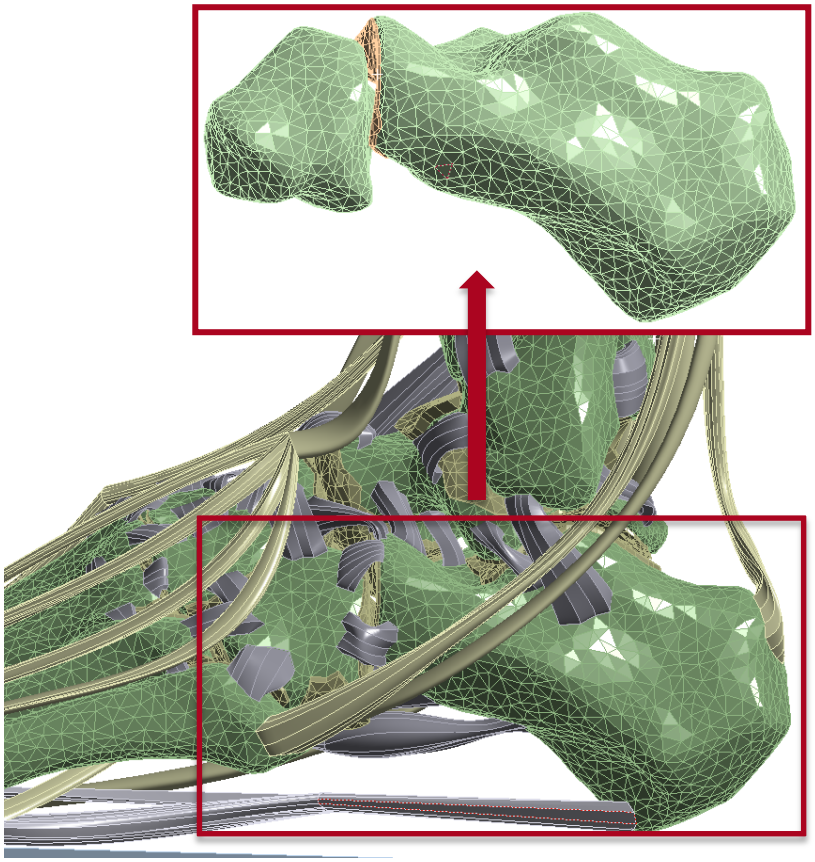

Figure 62: Diagram of where a frictionless contact was made on the cartilage layers of the calcaneocuboid joint in ANSYS Workbench

4. RESULTS

Using ANSYS APDL from the simulation described in Section 3.5, the first load step was solved. Since there were no forces applied to the model, there were no stresses or displacements in the results. In the second load step, an error occurred because of convergence problems (Figure 63).

```
*** WARNING ***                         CP =    3789.965   TIME= 14:32:35
The unconverged solution (identified as time 1 substep 999999) is
output for analysis debug purposes.  Results should not be used for
any other purpose.
```

Figure 63: ANSYS unconverged solution error message

Before the solution output the error message and ended the simulation, the second load step was able to solve 13 substeps. The results at that point were only output in order to debug the model and should not be considered a true representation of stresses. Figure 64 shows the equivalent stresses from the model at load step 2, substep 13. The figure only shows a few local areas with extremely high stresses suggesting problem areas in the model.

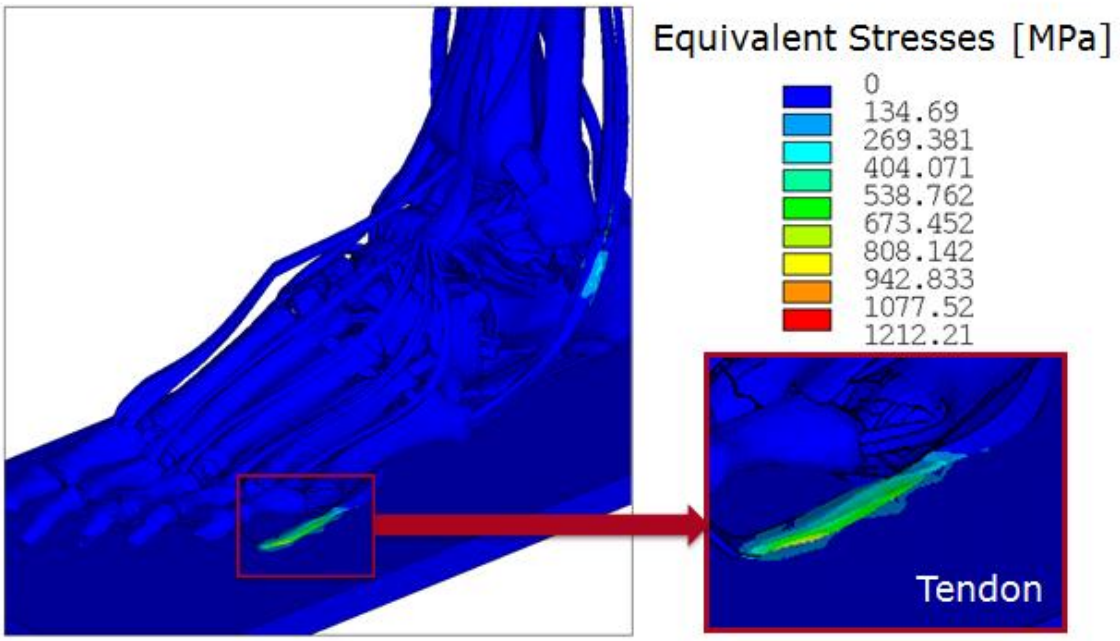

Figure 64: Equivalent stresses [MPa] for entire foot model in ANSYS APDL

In order to see if the simulation is close to replicating results of other studies, the values were filtered. Several studies show typical peak stresses on the bottom of a healthy foot ranging from 131 kPa to 231 kPa (Cheung, et al., May 2015; see also Wui, et al. Dec. 2011; Chen et al., 2001; Antunes et al., 2008). In ANSYS APDL, certain values of stresses can be displayed. The stress values, between 131 kPa and 231 kPa are displayed in green in Figure 65. The red values show stresses slightly higher i.e. up to 350 kPa. The figure below shows that the peak stress on the heel bone was approximately 318 kPa. All values larger than 350 kPa were displayed in gray.

Therefore, the plantar fascia and all other ligaments were experiencing large stresses when in contact with the ground. Figure 65 shows that the stresses on the inferior part of the heel were relatively close to the stresses reported in other studies.

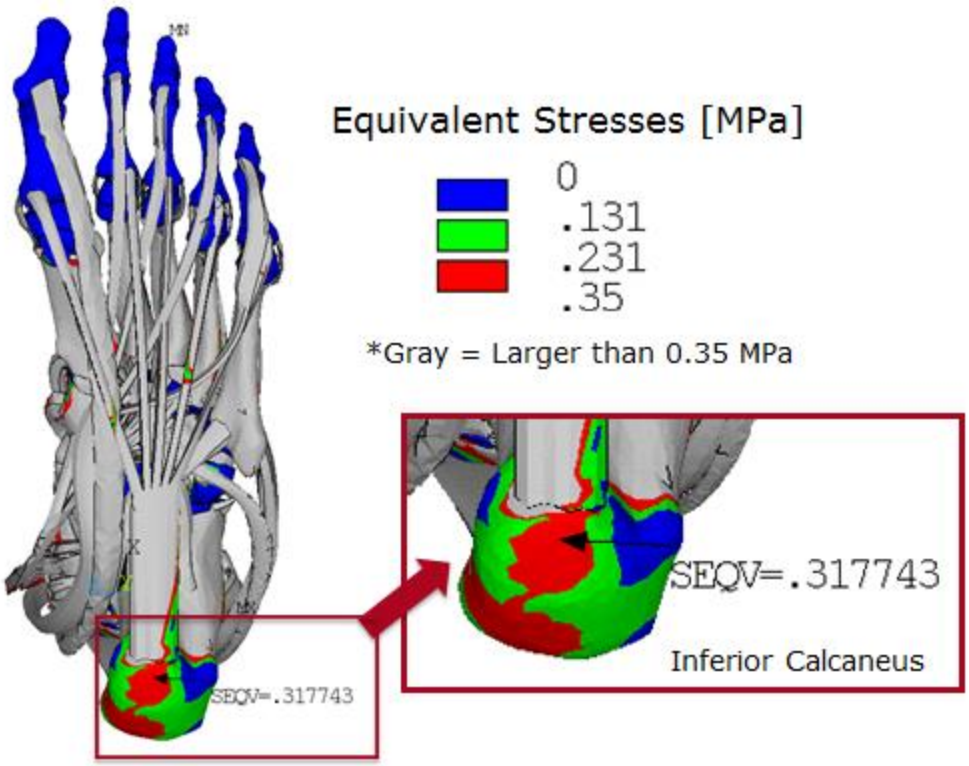

Figure 65: Equivalent stresses [MPa] on calcaneus (heel) using green color to represent the range of peak stresses of the calcaneus in research in ANSYS APDL

5. DISCUSSION AND FUTURE WORK

5.1 Finite Element Model Discussion

The value of creating a realistic foot geometry when setting up a finite element model offers great benefits, but some significant drawbacks. Benefits include a more realistic model, an opportunity for submodels, and less difficulty when changing loading or materials. Drawbacks include a lack of convergence using this software and hardware formulation, several hours of troubleshooting, and results that suggest unrealistic mechanical behavior and large stresses.

5.1.1 Finite Element Model Benefits

The overall goal to create an anatomically correct foot for a finite element model was achieved. The varying thicknesses of ligaments and tendons were modeled. The trabecular bone lying inside the cortical shell was successfully modeled from the CT scans. Although the entire model was not able to run, submodels could be made out of this complex model. ANSYS can easily suppress components to allow running of submodels. For example, a researcher could isolate a few bones and their respective ligaments, cartilage, and tendons to perform a focused study. ANSYS Workbench also makes it fairly simple to change forces, boundary conditions, and material properties. Changing material properties or locations of loading is a much faster process in a finite element model compared to changing these parameters when testing cadaveric parts on a mechanical test machine.

5.1.2. Finite Element Model Drawbacks

Unfortunately, the realistic finite element model of a foot that was prepared in this study has a few drawbacks. Changing only one contact to become frictionless and not converging to a solution represent major problems with the model. The model had over 200 contacts that should be frictionless contacts. The amount of time required to troubleshoot each contact pair is extensive ranging from weeks to months. The solve time of this model took hours to complete. Altering a few parameters in the model can take minutes, but determining how these changes affect convergence takes more time.

Another problem is that ligaments and tendons currently do not show true mechanical behavior as solid bodies. Ideally, ligaments and tendons act only in tension, but there is no solid element that can only act in tension. Between providing varying cross-sections and providing tension-only behavior, the tension-only behavior is more important to having the model provide accurate results.

As seen in the results from Figure 64, there are extremely high stresses on ligaments and tendons on the inferior portion of the foot. The high stresses are an artifact of the crushing of tissues on the bottom of the foot because there is no soft tissue being modeled. The elements of the inferior ligaments and tendons are undergoing unusually large shape deformations with large forces from the foot to create the artificially high stresses. Adding fat pads to the areas with high stresses would help alleviate the stresses.

5.3. Future Work

5.2.1. Model Adjustments for Convergence

In order to mitigate the drawbacks from the model's lack of convergence, a few tasks need to be performed. The suggestions are listed in order starting with the most important. The following suggestions are recommended for convergence: combining cartilage bodies, simplifying ligaments, adding spring ligaments to tendons, and adding fat pads and soft tissue.

5.2.1.1. Combine cartilage bodies

ANSYS Workbench contains geometry editing software called SpaceClaim. SpaceClaim is a powerful tool that is able to clean up and defeature geometry before entering the finite element model for meshing. As seen in Figure 66, the solid bodies that make up cartilage are all separate bodies based on the extrusions made in SolidWorks. The individual cartilage bodies that are joined together can be combined in SpaceClaim to look similar to Figure 67. Combining the individual bodies into one solid body will eliminate some unnecessary contacts within the cartilage bodies. Less contact pairs reduces the number of contact elements and nodes. Reducing contacts, elements, and nodes will significantly reduce solve-time.

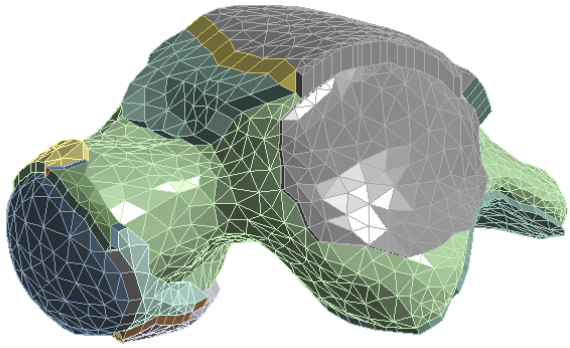

Figure 66: Talus bone with independent cartilage extrusions in ANSYS Workbench

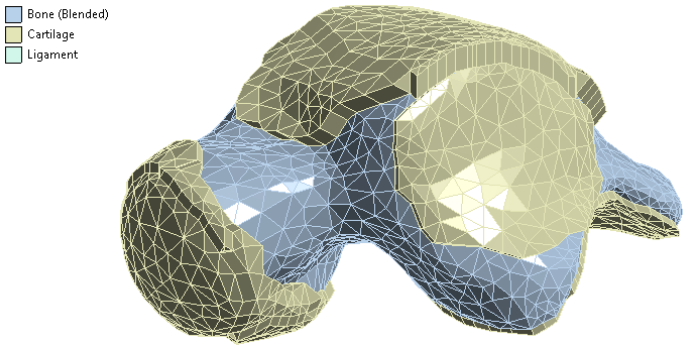

Figure 67: Talus bone with combined cartilage extrusions in ANSYS Workbench

To further reduce the solve-time associated with the cartilage bodies, the combined cartilage bodies can be simplified into surfaces. Reducing the solid bodies into surfaces can also be performed in SpaceClaim. After creating surfaces and importing the geometry into ANSYS Workbench, a thickness can be assigned to the surfaces to represent the cartilage thickness. ANSYS will mesh the surfaces with shell elements, which are computationally inexpensive in comparison to solid elements. The shell elements can be applied to the cartilage because the geometry is very thin in comparison to the area that the cartilage covers. Not only will this simplify the model further for convergence, but it will also reduce the solve-time.

5.2.1.2. Simplify ligaments

To restore the true tension-only mechanical behavior of ligaments, the ligaments need to be simplified from solid elements to truss elements. This can be done by removing each ligament and replacing the origin and insertion areas with a single node in the center of the cross-section. A LINK180 element can then be made connecting the origin node to the insertion node to represent the truss element (Figure 52). To restore some realistic features to the ligaments, an average cross-sectional area for each ligament can be used. Applying individual cross-sectional areas is still an improvement from other studies that will generally use only one cross-section to represent all ligaments.

Reducing each ligament solid body into two nodes and one element will significantly decrease the total amount of nodes and elements in the body. Reducing the node and element count will contribute to a faster solve-time. If some ligaments still need to retain their bending geometry, the lines can be discretized. Discretizing lines into separate elements can also restore variable cross-sections. The truss element can also be set to act only in tension, which rectifies the ligament's behavior.

5.2.1.3. Add spring elements to tendons

Similar to the ligaments, the tendons should also have a tension-only behavior. Unfortunately, tendons have a more complicated path to follow compared to the ligaments. The tendons should remain as solid elements, but spring elements need to be added to the model. Spring elements should connect from tendons to neighboring bones to keep the tendons in place. Tendons will remain in their respective load paths if a very stiff spring attaches to the bends of the tendons. At any point in the tendon where there is a bend or change in path, a spring element needs to be attached from that point to the closest bone. For example, a spring element would be made between the slight bend in the Achilles tendon and the tibia bone (Figure 68). A stiffness sensitivity study should be performed to determine the stiffness of the springs necessary to hold the tendons in place without creating artificial stress. Without this alteration, tendons will move in the path of least resistance and compromise their tension-only behavior.

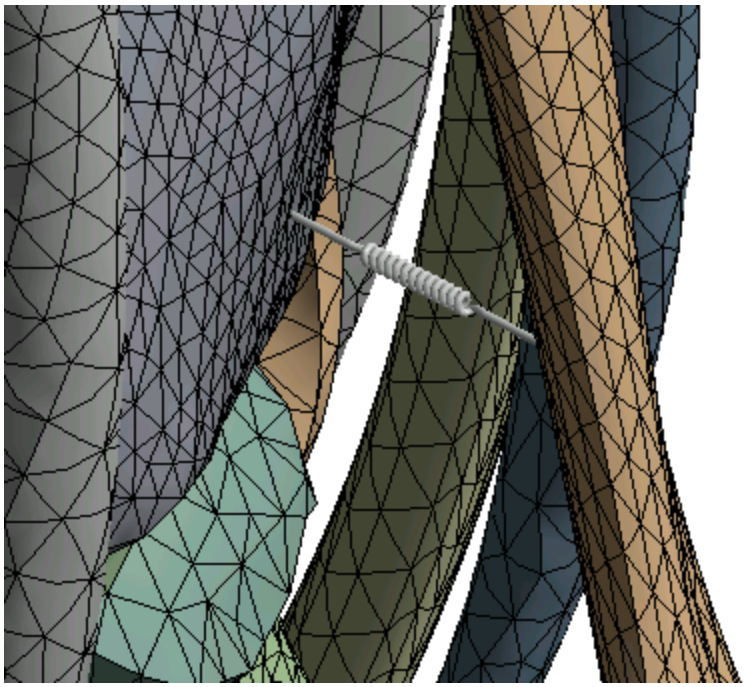

Figure 68: Spring element between posterior surface of tibia bone and Achilles tendon in ANSYS Workbench

5.2.1.4. Add fat pad

Adding a fat pad to the model can be a solution for alleviating high stresses on the bottom of the foot and for getting the model to converge. As seen in the results, there are unusually high stresses on the inferior ligaments and tendons in the foot. This is caused by the superior parts of the foot crushing the inferior ligaments and tendons into the ground support. Realistically, there are fat pads on the inferior part of the foot located at the sole and heel (Figure 69). The fat pads are thick pads of connective tissue that provide cushioning to alleviate friction, pressure, and gravitational forces. They also help shift the body weight so that it does not overwhelm other connective tissue (Pearl, 2017). Adding these fat pads to the model with realistic material properties will help alleviate the stresses in the inferior portions of the foot.

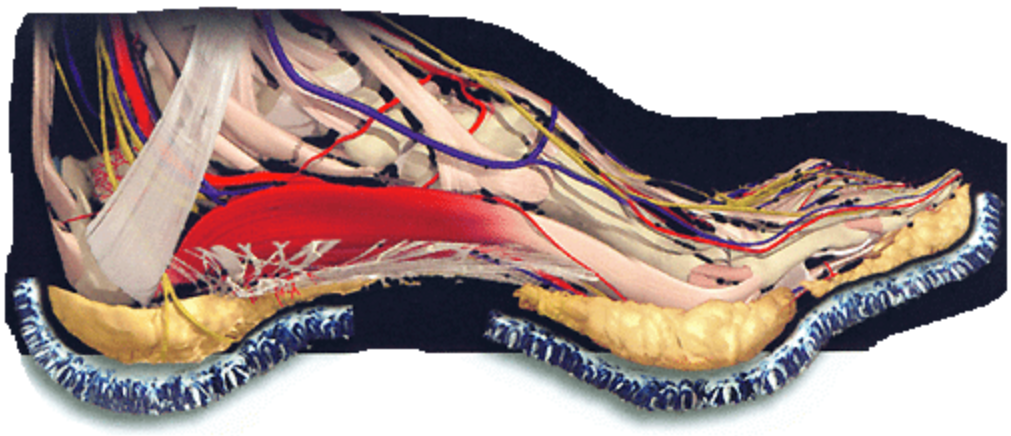

Figure 69: Fat pads on the sole and heel of the foot (Pearl, 2017)

5.2.1.5. Add soft tissue

The fat pads may help alleviate the stress, but there still remains a convergence issue due to contacts. Currently, the bones are all expected to interact with each other through frictionless contacts between cartilage bodies. As seen in the results, the nonlinear contact has a hard time understanding where to move in order to find contact between one joint. This problem can better be explained with a simple example.

Consider three bodies that can only move in one dimension. One body is fixed, one has a force applied, and the last is sitting in between the other two bodies (Figure 70). One can expect that Body 1 will move to the left, come into contact with Body 2, continue to move left, and finally come into contact with Body 3. The finite element method does not predict this simple hypothesis. Instead, there are mathematical problems because Body 2 is unconstrained and Body 1 doesn't know when the applied force will allow it to come into contact with Body 2.

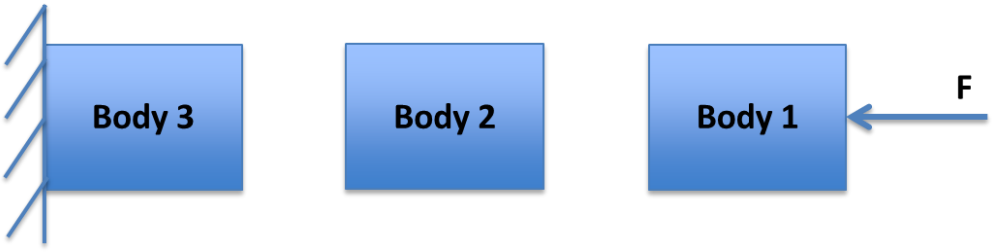

Figure 70: 1D Example – A. Three separate bodies in contact problem

Instead of creating the previous model setup, an analyst will set this example up using enforced displacements in several load steps. In the example, Body 2 will now be fixed and Body 1 will receive a displacement constraint to come into contact with Body 2 (Figure 71). Body 1 now understands how far to move in order to come into contact with Body 2.

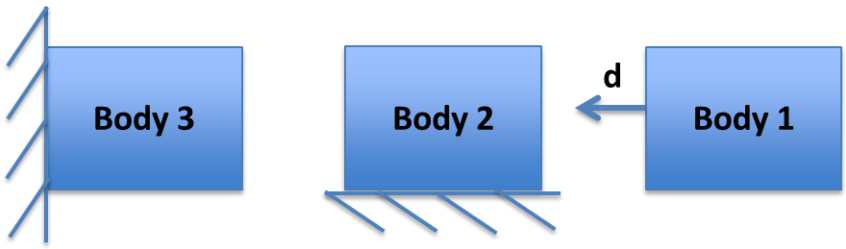

Figure 71: 1D Example – B. FEM Setup, Load Step 1

Once Body 1 and Body 2 come into contact with one another, the fixed constraint on Body 2 will be removed. Now, an enforced displacement will be applied to Body 1 and Body 2 to come into contact with Body 3 (Figure 72). Once all three bodies are finally in contact, a third load step is made in order to apply the original force (Figure 73).

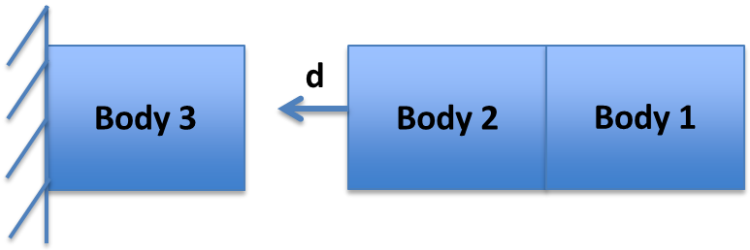

Figure 72: 1D Example – C. FEM Setup, Load Step 2

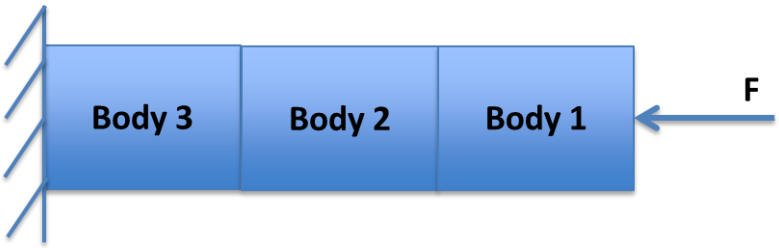

Figure 73: 1D Example – D. FEM Setup, Load Step 3

After understanding the difficulty with contact for a single degree of freedom problem, think about the complex foot model. The foot model has six degrees of freedom and no enforced displacements to keep everything in contact. There is only one force at the superior part of the foot to propagate throughout the bones. Therefore, another material like soft tissue could be added to force contact between all components.

Most of nonlinear contact can be removed by adding soft tissue to the body. Soft tissue can be added around and in between every bone, ligament, and tendon until forming the outer skin layer (Figure 74). Creating the soft tissue will eliminate any empty space currently in the model. Therefore, all outer elements of bones, ligaments, and tendons would share contact and be bonded to the soft tissue elements surrounding it. The only nonlinear contact left in the model is between the inferior part of the soft tissue and the ground support.

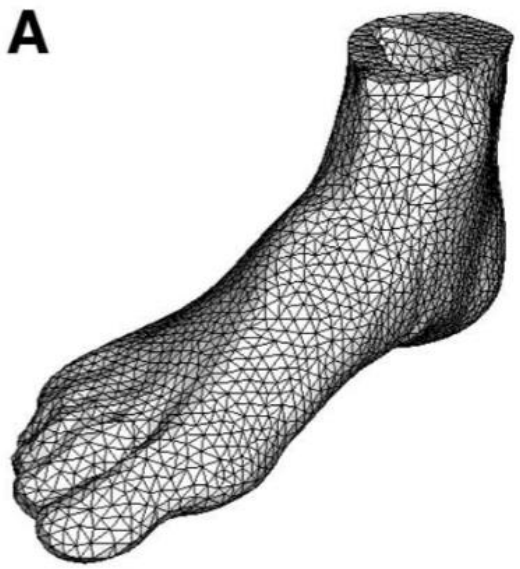

Figure 74: Soft tissue represented as tetrahedral elements in finite element model (Cheung & Zhang, 2005)

Including soft tissue in the model could greatly increase the possibility of convergence in the model, but there are some timely drawbacks. In order to create a realistic geometry of the soft tissue, the CT scans of the foot in the model would need to be used. This step would require going to the beginning of the process in order to add an accurate representation of the soft tissue. Also, the tibia and fibula were rotated in order to create a right angle with the ground support. Therefore, the soft tissue would not align with the current model and the soft tissue would also need to be altered. In conclusion, including soft tissue in the model would be the most time intensive step, but the final results could improve convergence.

5.2.2. Compare Results

After the model is able to run without showing unusually high stresses or convergence problems, the results will be compared with existing models. Results to compare include stresses on the inferior part of the foot and contact stresses between bones. The results should be compared to the other existing article that pertains to using a finite element model for Flatfoot analysis (Wang, et al., 2014). Stresses should be in the same range of values before simulating Flatfoot.

5.2.3. Simulate Flatfoot

After results look similar to other published articles, Flatfoot conditions can be simulated using the model. This includes attenuating tissue elements such as the spring ligament and the posterior tibial tendon in order to collapse the arch of the foot. A simple way to see how these tissues affect the foot is by removing them from the model and running the same analysis. Another method is reducing the strength of specific ligaments and tendons using the assigned material properties.

5.2.4. Simulate Osteotomies

After the symptoms of flatfoot are simulated properly and the arch collapses, the osteotomies can be simulated. Osteotomies to simulate include lateral column lengthening and cotton osteotomies. In order to create a space for the wedges, a sliver of elements in those areas can be deleted. The remaining elements will need to be cleaned up to meet a similar wedge shape. Then, the wedges will be inserted using a force to push the wedges into the slivered area and simulate the bone opening up to accept the wedge. Several wedge sizes will be simulated to see the effects of the wedge sizes. The lateral column lengthening will have wedges ranging from 6 to 12 mm thick. The cotton osteotomies will have wedges ranging from 5 to 8 mm thick. Analysis will be performed in order to see how the wedge sizes affect how the ankle rotates around the talar head and reforms an arch. Contact stresses will be obtained to see how the wedges affect the relationship between bones near the wedges.

6. CONCLUSION

Adult-Acquired Flatfoot is a complicated condition to correct because of the many malalignments in the foot. Finite element analysis provides an option to understand how the foot deforms and experiences stresses. In order to correct Flatfoot, one must understand normal deformation and stresses in a healthy foot.

A realistic model of a healthy foot was created using several software programs including 3D Slicer, 3-Matic, and SolidWorks. The model consisted of several tissues in the foot such as bone, cartilage, ligaments, and tendons. Unlike previous studies, the model contained cortical and trabecular bone as separate entities and ligaments and tendons were modeled as solid elements instead of truss elements. The tissues were represented as solid bodies in order to retain their true mechanical behavior due to their complex geometry.

After creating the realistic model, the geometry was imported into finite element software, ANSYS. In ANSYS, the model was assigned linear elastic material properties, boundary conditions, tendon loading, and contacts. To replicate the bones gliding on one another through cartilage, nonlinear frictionless contacts were created.

Inputting the model for solving resulted in convergence errors due to nonlinear contact. Abnormally large stresses were found on the inferior part of the foot due to ligaments and tendons being crushed by the stiff ground support. As the model was successfully seen as an anatomically correct representation of the foot and ankle, the model is not well designed for finite element analysis. Simplifications need to be made to the model before another simulation is performed. These simplifications include reducing detail of ligaments, adding spring elements to tendons, and adding fat pads and soft tissue. After a mixture of these simplifications are made and cause the simulation to converge, practical results will be obtained.

Once practical results are found for a healthy foot, the results can be compared to previous studies. After results are similar with other studies, the conditions of Flatfoot can be applied to the foot model. Osteotomies will be simulated on the Flatfoot model with different wedge sizes in order to see the effects of correcting the malalignments.

7. APPENDICES

7.1. APPENDIX A – List of Modeled Bones

Table 5: List of modeled bones

Section of Foot and Ankle	Modeled Bones
Leg	Tibia
	Fibula
Hindfoot	Calcaneus
	Talus
Midfoot	Medial cuneiform
	Intermediate cuneiform
	Lateral cuneiform
	Cuboid
	Navicular
Forefoot	1st Metatarsal
	Medial sesamoid
	Lateral sesamoid
	2nd Metatarsal
	3rd Metatarsal
	4th Metatarsal
	5th Metatarsal
	1st Proximal phalanx
	2nd Proximal phalanx
	3rd Proximal phalanx
	4th Proximal phalanx
	5th Proximal phalanx
	1st Distal phalanx
	2nd Distal phalanx
	3rd Distal phalanx
	4th Distal phalanx
	5th Distal phalanx

7.2. APPENDIX B – List of Modeled Ligaments

Table 6: List of modeled ligaments

No.	Ligament	Origin	Insertion
1	Anterior talofibular	Fibula	Talus
2	Anterior tibiofibular	Tibia	Fibula
3	Bifurcate (Calcaneocuboid part)	Calcaneus	Cuboid
4	Bifurcate (calcaneonavicular part)	Calcaneus	Navicular
5	Calcaneofibular	Calcaneus	Fibula
6	Cervical	Calcaneus	Talus
7	Deep anterior tibiotalar	Tibia	Talus
8	Deep posterior tibiotalar	Tibia	Talus
9	Dorsal calcaneocuboid	Calcaneus	Cuboid
10	Dorsal cubonavicular	Navicular	Cuboid
11	Dorsal cuneocuboid	Lateral cuneiform	Cuboid
12	Dorsal cuneonavicular 1	Navicular	Medial cuneiform
13	Dorsal cuneonavicular 2	Navicular	Intermediate cuneiform
14	Dorsal cuneonavicular 3	Navicular	Lateral cuneiform
15	Dorsal intercuneiform 1	Intermediate cuneiform	Lateral cuneiform
16	Dorsal intercuneiform 2	Medial cuneiform	Intermediate cuneiform
17	Dorsal intermetatarsal 1	Metatarsal 2	Metatarsal 3
18	Dorsal intermetatarsal 2	Metatarsal 3	Metatarsal 4
19	Dorsal intermetatarsal 3	Metatarsal 4	Metatarsal 5
20	Dorsal tarsometatarsal 1	Medial cuneiform	Metatarsal 1
21	Dorsal tarsometatarsal 2	Medial cuneiform	Metatarsal 2
22	Dorsal tarsometatarsal 3	Intermediate cuneiform	Metatarsal 2
23	Dorsal tarsometatarsal 4	Lateral cuneiform	Metatarsal 2
24	Dorsal tarsometatarsal 5	Lateral cuneiform	Metatarsal 3
25	Dorsal tarsometatarsal 6	Cuboid	Metatarsal 4
26	Dorsal tarsometatarsal 7	Cuboid	Metatarsal 5
27	Interosseous talocalcaneal	Talus	Calcaneus
28	Intersesamoid	Medial sesamoid	Lateral sesamoid
29	Lateral metatarso-sesamoid suspensory	Metatarsal 1	Lateral sesamoid
30	Lateral metatarsophalangeal 1	Metatarsal 1	Proximal phalanx 1
31	Lateral metatarsophalangeal 2	Metatarsal 2	Proximal phalanx 2
32	Lateral metatarsophalangeal 3	Metatarsal 3	Proximal phalanx 3
33	Lateral metatarsophalangeal 4	Metatarsal 4	Proximal phalanx 4
34	Lateral metatarsophalangeal 5	Metatarsal 5	Proximal phalanx 5
35	Lateral talocalcaneal	Talus	Calcaneus
36	Long plantar	Calcaneus	2^{nd} – 5^{th} Metatarsals
37	Medial metatarso-sesamoid suspensory	Metatarsal 1	Medial sesamoid
38	Medial metatarsophalangeal 1	Metatarsal 1	Proximal phalanx 1

39	Medial metatarsophalangeal 2	Metatarsal 2	Proximal phalanx 2
40	Medial metatarsophalangeal 3	Metatarsal 3	Proximal phalanx 3
41	Medial metatarsophalangeal 4	Metatarsal 4	Proximal phalanx 4
42	Medial metatarsophalangeal 5	Metatarsal 5	Proximal phalanx 5
43	Medial talocalcaneal	Talus	Calcaneus
44	Plantar cubonavicular	Navicular	Cuboid
45	Plantar cuneocuboid	Cuboid	Lateral cuneiform
46	Plantar cuneonavicular 1	Navicular	Medial cuneiform
47	Plantar cuneonavicular 2	Navicular	Lateral cuneiform
48	Plantar cuneonavicular 3	Navicular	Intermediate cuneiform
49	Plantar intercuneiform 1	Intermediate Cuneiform	Lateral cuneiform
50	Plantar intercuneiform 2	Medial cuneiform	Intermediate cuneiform
51	Plantar intermetatarsal 1	Metatarsal 4	Metatarsal 5
52	Plantar intermetatarsal 2	Metatarsal 3	Metatarsal 4
53	Plantar intermetatarsal 3	Metatarsal 2	Metatarsal 3
54	Plantar tarsometatarsal 1	Medial cuneiform	Metatarsal 1
55	Plantar tarsometatarsal 2	Lateral cuneiform	Metatarsal 3
56	Plantar tarsometatarsal 3	Cuboid	Metatarsal 5
57	Plantar tarsometatarsal 4	Medial cuneiform	Metatarsal 3
58	Plantar tarsometatarsal 5	Cuboid	Metatarsal 4
59	Plantar tarsometatarsal 6	Medial cuneiform	Metatarsal 2
60	Plantar tarsometatarsal 7	Metatarsal 3	Metatarsal 4
61	Posterior talofibular	Fibula	Talus
62	Posterior tibiofibular	Tibia	Fibula
63	Short plantar	Calcaneus	Cuboid
64	Spring (calcaneonavicular)	Calcaneus	Navicular
65	Superficial posterior tibiotalar	Tibia	Talus
66	Talonavicular	Talus	Navicular
67	Tibiocalcaneal	Tibia	Calcaneus
68	Tibionavicular	Tibia	Navicular
69	Tibiospring (anterior tibiotalar)	Tibia	Talus

7.3. APPENDIX C – List of Modeled Tendons

Table 7: List of modeled tendons

No.	Tendon	Origin	Insertion
1	Anterior tibialis	Interosseous membrane	Medial cuneiform, 1st Metatarsal
2	Posterior tibialis	Interosseous membrane	Navicular, Metatarsals 2-4
3	Flexor digitorum longus	Tibia	2nd – 5th Distal phalanges
4	Flexor hallucis longus	Fibula, Interosseous membrane	1st Distal phalanx
5	Achilles	Soleus and calf muscles	Calcaneus
6	Peroneus longus	Fibula, Intermuscular septa	Medial cuneiform, 1st Metatarsal
7	Peroneus brevis	Fibula, Intermuscular septa	5th Metatarsal
8	Extensor hallucis longus	Fibula, Interosseous membrane	1st Distal phalanx
9	Extensor digitorum longus	Tibia, Fibula, Interosseous membrane, Intermuscular septa	2nd – 5th Distal phalanges

7.4. APPENDIX D – Model Images courtesy of ANSYS, Inc. Version 17.0

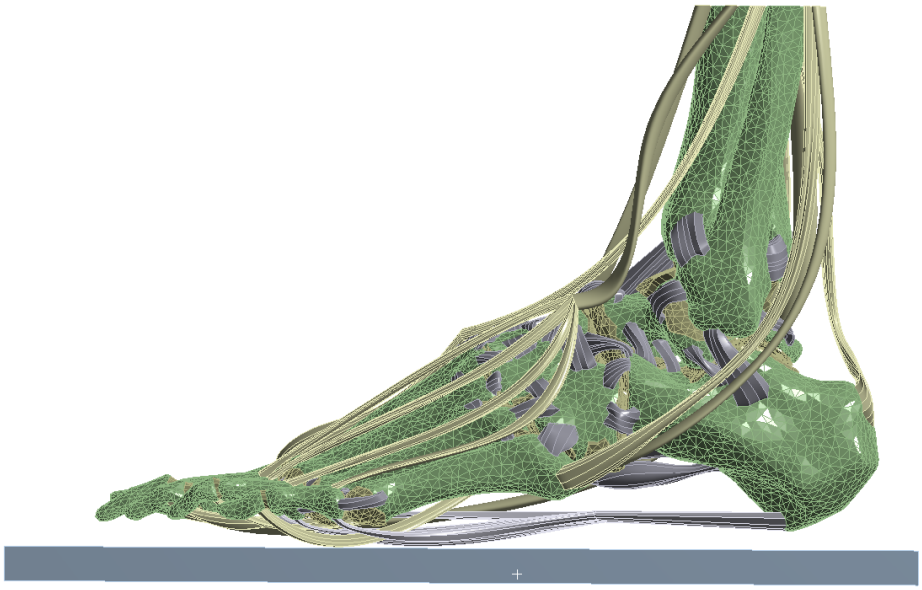

Figure 75: Lateral viewpoint of foot model

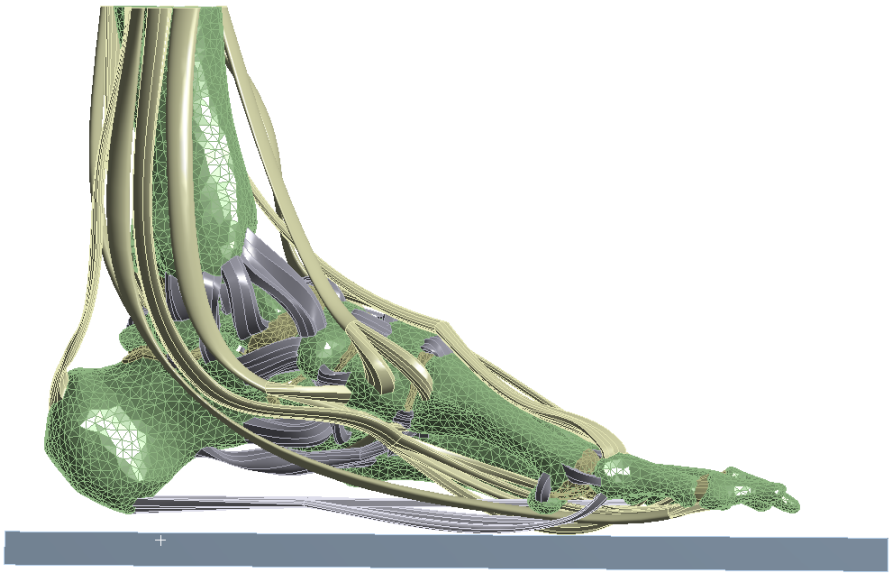

Figure 76: Medial viewpoint of foot model

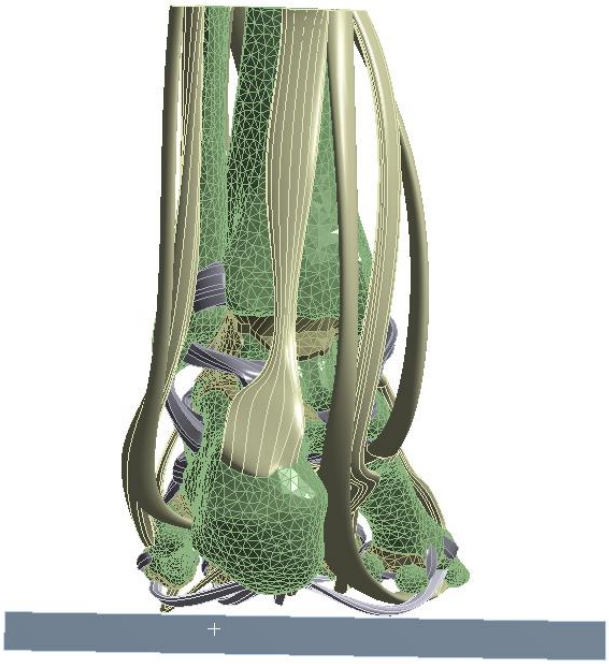

Figure 77: Posterior viewpoint of foot model

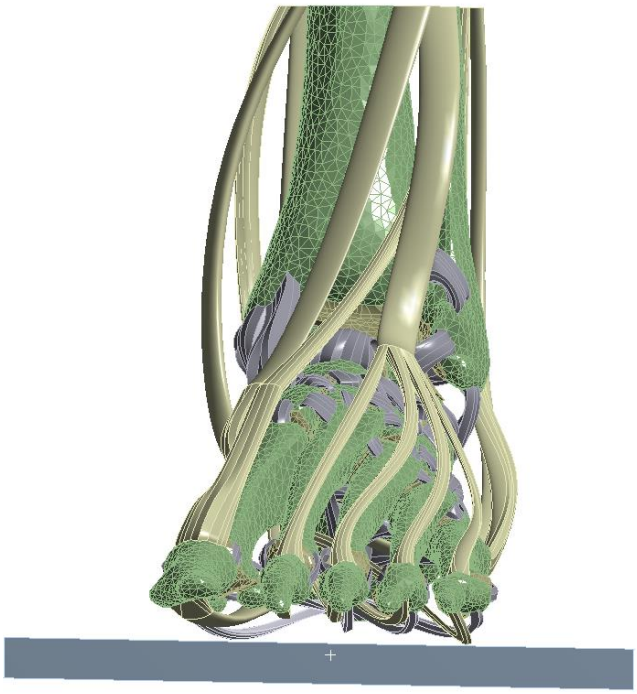

Figure 78: Anterior viewpoint of foot model

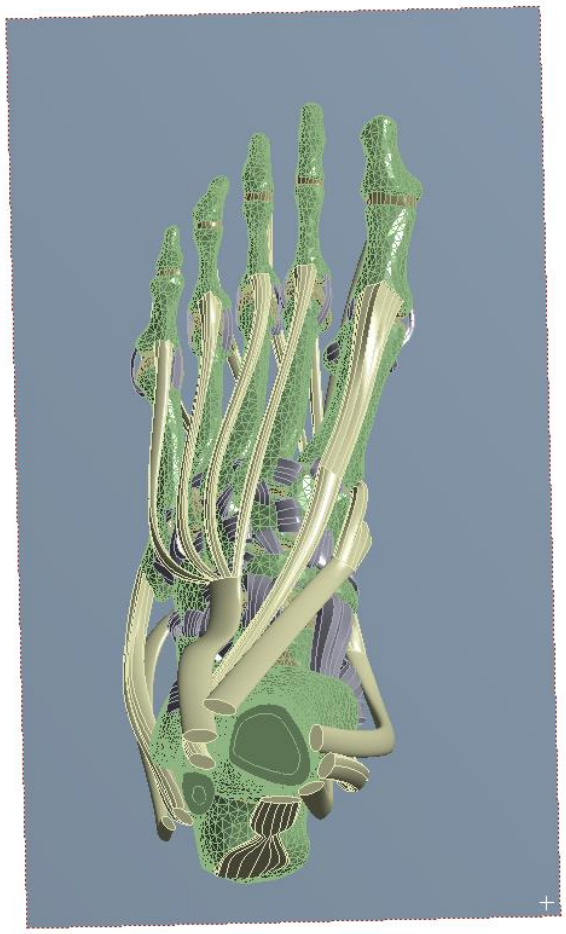

Figure 79: Superior viewpoint of foot model

REFERENCES

3D Slicer. (n.d.). [Computer software].

3-matic. (n.d.). Materialise. [Computer software].

Achilles Tendon Problems. (n.d.). Retrieved August 06, 2017, from http://www.houstonmethodist.org/orthopedics/where-does-it-hurt/foot/achilles-tendon-problems/

Anatomy of the Foot. (n.d.). Retrieved July 29, 2017, from http://www.arthritis.org/about-arthritis/where-it-hurts/foot-heel-and-toe-pain/foot-anatomy.php

ANSYS, Inc., Release 17.0 Documentation (n.d.)., Retrieved from http://www.ansys.com/

Antunes, P. J., Dias, G. R., Coelho, A. T., Rebelo, R., & Pereira, T. (2008). Non-Linear Finite Element Modelling of Anatomically Detailed 3D Foot Model. Report Paper, 1-11.

Arangio, G. A., & Salathe, E. P. (2002). A Biomechanical Model of the Foot: The Role of Muscles, Tendons, and Ligaments. *Journal of Biomechanical Engineering, 124*(3), 281-287. doi:10.1115/1.1468865

Ashkan. (2014, January 21). 1D Spring Element FE Code. Retrieved August 06, 2017, from https://www.mathworks.com/matlabcentral/fileexchange/45155-1d-spring-element-fe-code

Bernal Covarrubias, R.R. (2015). *Biomechanical Assessment of a Human Joint Under Natural and Clinically Modified Conditions: The Shoulder.* Retrieved from the University of Arizona University Libraries http://hdl.handle.net/10150/556975

Blahd, W., & Fu, F. (2015, May 22). Cartilage. Retrieved August 06, 2017, from http://www.webmd.com/first-aid/cartilage

Boss, A. P., & Hintermann, B. (2002). Anatomical Study of the Medial Ankle Ligament Complex. *Foot & Ankle International, 23*(6), 547-553. doi:10.1177/107110070202300612

Campagne, D. (2014, December). Ankle Sprains. Retrieved August 06, 2017, from http://www.merckmanuals.com/professional/injuries-poisoning/fractures,-dislocations,-and-sprains/ankle-sprains

Campbell, K. J., Michalski, M. P., Wilson, K. J., Goldsmith, M. T., Wijdicks, C. A., Laprade, R. F., & Clanton, T. O. (Apr. 2014). The Ligament Anatomy of the Deltoid Complex of the Ankle: A Qualitative and Quantitative Anatomical Study. *The Journal of Bone and Joint Surgery-American Volume, 96*(8). doi:10.2106/jbjs.m.00870

Chen, W., Tang, F., & Ju, C. (2001). Stress distribution of the foot during mid-stance to push-off in barefoot gait: a 3-D finite element analysis. *Clinical Biomechanics*, *16*(7), 614-620. doi:10.1016/s0268-0033(01)00047-x

Chen, Y., Chang, C., Li, C., Chang, C., & Lin, C. (Sep. 2014). Finite Element Analysis of Plantar Fascia During Walking. *Foot & Ankle International, 36*(1), 90-97. doi:10.1177/1071100714549189

Cheung, J. T., Zhang, M., Leung, A. K., & Fan, Y. (May 2004). Three-dimensional finite element analysis of the foot during standing—a material sensitivity study. *Journal of Biomechanics, 38*(5), 1045-1054. doi:10.1016/j.jbiomech.2004.05.035

Cheung, J. T., & Zhang, M. (2005). A 3-dimensional finite element model of the human foot and ankle for insole design. *Archives of Physical Medicine and Rehabilitation*, *86*(2), 353-358. doi:10.1016/j.apmr.2004.03.031

Chimenti, R. L., Tome, J., Hillin, C. D., Flemister, A. S., & Houck, J. (Apr. 2014). Adult-acquired flatfoot deformity and age-related differences in foot and ankle kinematics during the single-limb heel-rise test. *Journal of Orthopaedic and Sports Physical Therapy, 44*(4), 283-290. doi:10.2519/jospt.2014.4939.

Chiro, M. (2013, February 12). The Shock Absorbers of the Spine. Retrieved August 06, 2017, from http://drmchiro.blogspot.com/2013/02/the-shock-absorbers-of-spine.html

Cohen, Z. A., Mccarthy, D. M., Kwak, S., Legrand, P., Fogarasi, F., Ciaccio, E. J., & Ateshian, G. A. (1999). Knee cartilage topography, thickness, and contact areas from MRI: in-vitro calibration and in-vivo measurements. *Osteoarthritis and Cartilage, 7*(1), 95-109. doi:10.1053/joca.1998.0165

Compact bone. (n.d.). Retrieved August 06, 2017, from https://www.britannica.com/science/compact-bone

Cotton, F. J. (1936). Foot Statics and Surgery. New England Journal of Medicine, 214(8), 353-362. doi:10.1056/nejm193602202140804

Crowninshield, R. D., & Nakamura, S. (1981). An analysis of soft tissue loading in the foot. *Journal of Biomechanics, 14*(7), 492. doi:10.1016/0021-9290(81)90128-7

Explaining Spinal Anatomy. (n.d.). Retrieved August 06, 2017, from http://www.sandiego-spine.com/subject.php?pn=spinal-anatomy-024

Fitzgordon, J. (2016, August 01). The Weight Bearing Bones of the Forearm and Shin. Retrieved August 06, 2017, from https://corewalking.com/weight-bearing-bones-forearm-shin/

Golanó, P., Vega, J., Leeuw, P. A., Malagelada, F., Manzanares, M. C., Götzens, V., & Dijk, C. N. (2010). Anatomy of the ankle ligaments: a pictorial essay. *Knee Surgery, Sports Traumatology, Arthroscopy, 18*(5), 557-569. doi:10.1007/s00167-010-1100-x

Jeelani, M. (2015, December 19). Linear Spring as a Finite Element and its Calculations. Retrieved August 06, 2017, from https://aerospaceengineering.aero/linear-spring-as-a-finite-element-and-its-calculations/

Konstantakos, M. E. (2016, May 10). What Is Cartilage? Retrieved August 06, 2017, from https://www.arthritis-health.com/types/joint-anatomy/what-cartilage

Laborde, J. M. (2010, May 01). Tendon Lengthening for Neuropathic Foot Problems. Retrieved August 06, 2017, from https://www.healio.com/orthopedics/journals/ortho/2010-5-335/%7B6470f847-9e33-4542-8b27-1ea0c1dd8c73%7D/tendon-lengthening-for-neuropathic-foot-problems

Latt, D. (2017, May 7). Optimization of osteotomies for flatfoot correction using finite element analysis. Lecture presented at Paragon 28 Presentation in Denver, Colorado.

Maganaris, C. N., & Paul, J. P. (Nov. 1999). In vivo human tendon mechanical properties. *Journal of Physiology, 521*(1), 301-313. doi:10.1111/j.1469-7793.1999.00307.x

Mahadevan, V., et al. (n.d.). Interactive foot & ankle. Primal Pictures. [Computer software].

Mudgal, P. (n.d.). Meary's angle | Radiology Reference Article. Retrieved July 29, 2017, from https://radiopaedia.org/articles/mearys-angle

Netter, F. H., & Colacino, S. (1997). *Atlas of human anatomy*. East Hanover, NJ: Navartis.

Northcoast Footcare. (n.d.). Retrieved August 06, 2017, from http://www.northcoastfootcare.com/pages/Foot-and-Ankle-Anatomy.html

OrthoAnswer. (2012, August 6). Flatfeet. Retrieved August 06, 2017, from http://www.orthoanswer.org/foot-ankle/flatfeet/index.html

Ozen, M., Sayman, O., & Havitcioglu, H. (2013). Modeling and Stress Analyses of a Normal Foot-Ankle and A Prosthetic Foot-Ankle Complex. *Acta Bioengineering and Biomechanics, 15*(3), 19-27.

Paragon 28. (n.d.). Orthopedic Implants | Foot & Ankle Bone Implants. Retrieved August 06, 2017, from http://www.paragon28.com/

Pearl, J. (2017, March 05). Fat Pad Atrophy of the Foot. Retrieved July 29, 2017, from https://www.mortonsneuroma.com/fat-pad-atrophy-foot/

Peltonen, J., Cronin, N. J., Avela, J., & Finni, T. (2010). In vivo mechanical response of human Achilles tendon to a single bout of hopping exercise. *Journal of Experimental Biology, 213*(8), 1259-1265. doi:10.1242/jeb.033514

Pes Cavus. (2016, August 14). Retrieved August 06, 2017, from http://uwmsk.org/footalignment/doku.php?id=pes_cavus

Qiu, T., Teo, E., Yan, Y., & Lei, W. (Dec. 2011). Finite Element Modeling of A 3D Coupled Foot-Boot Model. *Medical Engineering & Physics*, *33*(10), 1228-1233.

Rose, M. (2017, June 28). Regional Biomechanics Ankle Joint & Foot. Retrieved August 06, 2017, from http://slideplayer.com/slide/6351583/

SolidWorks (Version 2012) [Computer software]. (n.d.).

Somastruct. (n.d.). Arches of the Foot. Retrieved August 06, 2017, from https://www.somastruct.com/arches-of-the-foot/

Sorrento, D. D. (n.d.). Ankle Joint Anatomy and Osteoarthritis. Retrieved July 29, 2017, from https://www.arthritis-health.com/types/osteoarthritis/ankle-joint-anatomy-and-osteoarthritis

Spyrou, L. A., & Aravas, N. (June 2011). Muscle-driven finite element simulation of human foot movements. *Computer Methods in Biomechanics and Biomedical Engineering, 15*(9), 925-934. doi:10.1080/10255842.2011.566564

Takano, J. (2014). Health Risks of Flat Feet and How You Can Prevent It. Retrieved August 06, 2017, from https://www.pyroenergen.com/articles12/flat-feet-risks.htm

Wang, Z., Imai, K., Kido, M., Ikoma, K., & Hirai, S. (2014). A Finite Element Model of Flatfoot (Pes Planus) for Improving Surgical Plan. International Conference of the IEEE Engineering in Medicine and Biology Society. doi:10.1109/embc.2014.6943723